UNIVERSITY OF GHANA

SCHOOL OF ENGINEERING SCIENCES

SYNTHESIS AND APPLICATION OF PURE AND MODIFIED TiO_2 FOR PHOTOCATALYTIC REMEDIATION OF FRACTIONATED CRUDE OIL.

BY

SELASSIE GBOGBO

(10599055)

A THESIS SUBMITTED TO THE SCHOOL OF GRADUATE STUDIES

IN PARTIALFULFILMENT OF THE AWARD OF DEGREE OF

MASTER OF PHILOSOPHY IN MATERIALS SCIENCE AND

ENGINEERING

DEPARTMENT OF MATERIALS SCIENCE AND ENGINEERING

2018

SCHOOL OF ENGINEERING SCIENCES

SYNTHESIS AND APPLICATION OF PURE AND MODIFIED TiO_2 FOR PHOTOCATALYTIC REMEDIATION OF FRACTIONATED CRUDE OIL.

BY

SELASSIE GBOGBO

(10599055)

A THESIS SUBMITTED TO THE SCHOOL OF GRADUATE STUDIES

IN PARTIALFULFILMENT OF THE AWARD OF DEGREE OF

MASTER OF PHILOSOPHY IN MATERIALS SCIENCE AND

ENGINEERING

DECLARATION

ACKNOWLEDGEMENTS

I am grateful to God whose I am and whom I serve for the supply of grace to be able to go through the programme and to put this document together.

I express my profound gratitude and appreciation to my supervisors, Dr. Emmanuel Nyankson and Dr. Benjamin Agyei-Tuffour for their guidance, patience, dynamism and motivation that has helped me to complete this research work successfully. I really appreciate the way you both guided me on how to access relevant materials for the research work.

I am also indebted to Most Rev. Titus Awotwi-Pratt, the presiding Bishop of the Methodist Church Ghana (MCG), Rt. Rev. Kwame Baffour Kyei, Bishop of the Akyem Oda Methodist Church, Very Rev. Kwame Boateng, Synod Secretary Akyem Oda MCG, Dr. Johnson Yeboah Gyekye, former Lay Chairman and the entire MCG, whose encouragement and support saw me enrolling in the programme and subsequently completing this research work. I am sincerely grateful to my mother, Miss Cecilia Asare Donkor and father Mr. Albert Kofi Gbogbo who supported me in cash and kind for me to come this far. I really appreciate the support and sacrifice of my beloved wife, Gloria and our three wonderful kids; Teras, Judah and Peniela. Thank you very much for the faith you have in me.

Special thanks go to the following people for the various ways they all supported to bring me this far, Dr. Lucas Damoah and all the Lecturers of the Department of Materials Science and Engineering, Very Rev. Dela Gator Sackey, Very Rev. Solomon Bruce, Miss Esinam Homuame, Miss Amelda Adwoa Appau, Miss Davina Appau, Mrs. Harriet Adu-Amoah, Dr. Mrs. Ellen Antwi-Adjei, Mr. Eric Anku, Mr. John Perry Aggrey, , Mr. Michael Ayesu, Mr. Ebenezer Addo, Mr. and Mrs. Awuakye, Mr. and Mrs. Kwesi and Benita Lois Amanor, Mrs. Madeline Nartey, Mrs. Olivia Parker-Langdon, Winnifred Nsiah, Mr. Samuel Owusu-Atuah, Shadrach and Uncle Ben of Biotech Lab, Mrs. Grace Karikari Arkorful and Mrs. Gloria

Pokuaa Manu of the Materials Lab, UG, Legon. I again appreciate the members of the Chaplaincy Committee of Attafuah Senior High and Technical School as well as members of the Calvary Methodist Church, Akyem Oda Nkwantanum. Without you the completion of this work would have been extremely difficult if not impossible.

I am indeed grateful to God for the opportunity to have been in the midst of great individuals who graced the MPhil Materials Science and Engineering Class of University of Ghana 2016 – 2018 academic year; Lois, Esther, Marfo, Takyi (Apostle), Theo, Amartey, Nii Arday. I was privileged to meet such great minds. The African Materials Research Society - University of Ghana Chapter (AMRS-UG Chapter) members and patrons are also acknowledged for the motivation and support. I am finally thankful to the Very Reverend Professor Kwabena Asamoah-Gyadu my mentor whose life and works have always inspired and challenged me in life.

DEDICATION

This work is dedicated to my beautiful wife Mrs. Gloria Gbogbo and our three wonderful children Teras Adwoa Nyamekye Benewa Gbogbo, Judah Papa Albert Gbogbo and Peniela Maame Dufie Gbogbo for their sacrifices and understanding of the demands of higher education.

TABLE OF CONTENTS

LIST OF FIGURES

LIST OF TABLES

LIST OF ACRONYMS AND ABBREVIATIONS

DCM	Dichloromethane
FTIR	Fourier Transform Infra-Red
SEM	Scanning Electron Microscopy
EDX	Energy Dispersive X-ray
XRD	X-Ray Diffraction
DRS	Diffuse Reflectance Spectroscopy
DSC	Differential Scanning Calorimetry
TGA	Thermogravimetric Analyses
UV-Vis	Ultraviolet -Visible
GC/MS	Gas Chromatography Mass Spectrometry
Fe-TiO_2+Aromatics (Sun)/ (UV)/ (Vis)	Mixture of Fe-TiO_2 and bulk Aromatics fraction of crude oil that has under gone four hours irradiation of sunlight (sun)/UV light (UV)/visible light (Vis).
Fe-TiO_2+Asphaltenes (Sun)/ (UV)/ (Vis)	Mixture of Fe-TiO_2 and bulk Asphaltenic fraction of crude oil that has under gone four hours irradiation of sunlight (sun)/UV light (UV)/visible light (Vis).
Fe-TiO_2+Paraffins (Sun)/ (UV)/ (Vis)	Mixture of Fe-TiO_2 and bulk Paraffinic fraction of crude oil that has under gone four hours irradiation of sunlight (sun)/UV light (UV)/visible light (Vis).
TiO_2+Aromatics (Sun)/ (UV)/ (Vis)	Mixture of TiO_2 and bulk Aromatics fraction of crude oil that has under gone four hours irradiation of sunlight (sun)/UV light (UV)/visible light (Vis).
TiO_2+Asphaltenes (Sun)/ (UV)/ (Vis)	Mixture of TiO_2 and bulk Asphaltinic fraction of crude oil that has under gone four hours irradiation of sunlight (sun)/UV light (UV)/visible light (Vis).
TiO_2+Paraffins (Sun)/ (UV)/ (Vis)	Mixture of TiO_2 and bulk Paraffinic fraction of crude oil that has under gone four hours irradiation of sunlight (sun)/UV light (UV)/visible light (Vis).
Nil+Aromatics (Sun)/ (UV)/ (Vis)	Bulk aromatics fraction of crude oil without photocatalyst that has under gone four hours irradiation of sunlight (sun)/UV light (UV)/visible light (Vis).

Nil+Asphaltenes (Sun)/ (UV)/ (Vis)	Bulk asphaltenic fraction of crude oil without photocatalyst that has under gone four hours irradiation of sunlight (sun)/UV light (UV)/visible light (Vis).
Nil+Paraffins (Sun)/ (UV)/ (Vis)	Bulk paraffinic fraction of crude oil without photocatalyst that has under gone four hours irradiation of sunlight (sun)/UV light (UV)/visible light (Vis).
DCM+Aromatics	Mixture of DCM and aromatics bulk fraction of crude oil.
DCM+Asphaltenes	Mixture of DCM and asphaltenic bulk fraction of crude oil.
DCM+Paraffins	Mixture of DCM and paraffinic bulk fraction of crude oil.
TTIP	Titanium Isopropoxide

ABSTRACT

Oil spills have been a major source of concern due its harmful effect on the environment. To reduce the effect of oil spills, new remediation strategies need to be developed whiles enhancing the efficiency of existing remediation ones. In this study, the potential of TiO_2 and its modified form (Fe-TiO_2) as a stand-alone or as an add-on remediation strategy was explored. This was carried out by accessing the how TiO_2 and Fe-TiO_2 photodegrades crude oil fractions (aromatics, paraffins, asphalthenes) under sunlight, visible (400W) and UV light with four (4) hours irradiation time. The TiO_2 and the Fe-TiO_2 used were synthesized with the mild hydrothermal method and characterized with XRD, UV-Vis, DRS, SEM, EDX, TGA, DSC and FTIR. These characterization techniques confirmed the production of the anatase phase TiO_2 and Fe-TiO_2 with estimated bandgap of 3.12 eV and 2.90eV, respectively. The Debye Scherrer's equation was used to compute the crystallite size from the XRD patterns as 4.10 nm and 3.85 nm for TiO_2 and Fe-TiO_2, respectively.

The photodegradation experiments on the aromatics, paraffins and asphalthenes showed that Fe-TiO_2 is better at degrading the fractions than TiO_2 under visible light and sunlight irradiation. These conclusions were arrived at from the analysis of the photoproducts using UV-Vis, FTIR and GC/MS. The GC/MS spectra showed the formation of new compounds, diminishing in the concentration of existing compounds and the disappearance of existing compounds. It was revealed that, photocatalysis is effective in remediating aromatics than asphaltenes and paraffins. The results from the study showed the potential of photo-remediation as a stand-alone or add-on oil spill response strategy.

CHAPTER ONE

1.0 INTRODUCTION

Oil discoveries are always met with intense joy and celebration since it brings major economic boom to the nations concerned. No wonder the discovery of oil in commercial quantities in Ghana was met with pomp and pageantry. Again, oil finds its usefulness in all sectors of every country's economy. It finds it use in the production of power and electricity, transportation, industries; fishing and agriculture just to mention a few. The above notwithstanding, the oil industry comes with its attendant problems that oil producing countries have to contend with. Crude oil impacts negatively on the Earth's biosphere, destroying the ecosystems through the spill of oils.

Even though exploitation fields in Ghana started not long ago, the attendant challenges of spillage have already started. Oil spills which mostly take place in the marine environment have ripple effect on the economy. When marine life is affected, there are deleterious consequences on nutrition, health and many more. The survival of the fisher folks is also affected. Again, the water lines of the marine environment which serve as recreation centers and tourist sites are destroyed by oil spills. The aggregated effect of all these is that the importance of the oil industry to the economy is not achieved.

Therefore, the need to safeguard the environment against oil spills cannot be achieved entirely by the remediating measures that have been adopted to deal with the menace. The present remediating measures include the use of chemical dispersants, mechanical containment with booms and collection, the in situ burning of contained oil on the seas and the use of biological agents to aid degradation and sorbent materials. Even though these measures have achieved significant remediation effects; there are existing teething problems

with many of their inventions. For instance, the chemical dispersants are relatively expensive and also have toxic effects on the environment [1].

Therefore, in this work, the potential of photocatalyst in degrading oil spills in the marine environments is explored. Common photocatalysts such as ZnO, SnO_2, ZrO_2, TiO_2 and CuO have been reported as effective in the photodegradation of different compounds. Among the mentioned photocatalysts, TiO_2 holds greater potential to photodegrade due to its desirable characteristics such as high chemical and thermal stability, tunable band gap and their availability in greater quantities [2-11].

When modified through doping, the TiO_2 optical properties are enhanced and therefore absorb radiation in both the ultraviolet and visible spectrum and this improves the photoabsorbance and consequently the photodegradation of pollutants are greatly enhanced [10, 11]. Hence in this work, Fe dopants was added to a mild hydrothermally synthesized TiO_2 and characterized. The pristine and modified TiO_2 was contacted with crude oil fractions under visible and ultraviolet light. The degradation rates as well as the photoproducts formed were examined. The findings were discussed to ascertain the potential of TiO_2 and its modified forms as reliable photodegradable catalysts.

1.1 RESEARCH STATEMENT/ANALYSIS OF THE PROBLEM AND HYPOTHESIS

The incidence of oil spills and its attendant challenges in the environments have always aroused media and political uproar, on the nation's response to oil spills. It has been observed that water dissolvable organic compounds from spilled oil remain in the ocean causing havoc to the marine environment with ripple effects on the economies and health of the residents in the spilled area. The remediation measures currently available have not completely dealt with the menace of oil spill. As an example, the most widely accepted oil spill remediation strategy; chemical dispersant has been reported to be toxic to aquatic species. Biodegradation

which occurs right after chemical dispersant application is very effective at degrading paraffinic component of crude oils. Current research has reported that, biodegradation is less effective in degrading water soluble aromatic components in crude oils. Hence the aromatic components remain in the ocean column for even decades after oil spillage. A remediation strategy that is effective in degrading all the components in crude oil is needed. Photocatalysis has been reported to be an effective way of degrading water-soluble pollutants such as dyes, pesticides and pharmaceuticals. Since crude oil is made up of different components, it is hypothesized that photocatalysis can be used to photodegrade the various fractions in crude oil resulting in the remediation. TiO_2 which is one of the most chemically stable photocatalyst will be the right choice for such a fundamental study. However, TiO_2 is only active in the UV region of the electromagnetic spectrum. Hence modification of TiO_2 would be required to make it active in the visible light region. This will be achieved by doping TiO_2 with Fe.

1.2 AIMS AND OBJECTIVES

The aim of this research is to assess the remediation effects of pure and modified TiO_2 photocatalysts on the photodegradation of crude oil in spill environments.

The objectives of the study include the following:

- Synthesize TiO_2 and Fe-TiO_2 photocatalyst,
- Fractionate crude oil into various components,
- Examine the potential of the synthesized photocatalyst in degrading the various fractions of the crude oil,
- Identify the photoproducts for the crude oil degradation.

1.3 SCOPE OF THE STUDY

Pristine and modified TiO_2 photocatalysts were synthesized and used to photodegrade components of crude oil. This project will help in the remediation of oil spills using sunlight.

This report consists of five chapters; introduction, literature review, materials and methods, results and discussions and the final chapter which will include the conclusions, recommendations and the references.

CHAPTER TWO

2.0 LITERATURE REVIEW

2.1.0 CRUDE OIL

Crude oil is formed by heating at high temperatures and pressure living materials which comes from heavy layer of sediments over a long period of time. The present crude oils being exploited come from the left overs of ancient photosynthetic organisms and heterotrophic plankton that lived at the lowest part of Oceans and Lakes [12].

Crude oil or petroleum as referred to, is a liquid located within the earth which is a mixture of organic compounds and scraps of metal [12, 13]. The main constituents of crude oil are formed from hydrocarbons having a composition that varies from 50 - 97 %. Nitrogen and oxygen (non-metals) found in crude oils make up 6 - 10%, whereas metals like copper, iron, vanadium and nickel make up for less than 1 % [12]. Crude oils may exist in different colours; colourless or pale yellow to red, green or the most common dark brown to black. Crude oils with different coloration are shown in Figure 2.1 below. It must be stated that no two crude oils are the same and they derive their uniqueness from their formation [14].

Figure 2. 1 Images of crude oils showing their different colorations[15]

Crude oil can be grouped into four bulk fractions based on their molecular weight and their separation mechanisms. These are saturates, aromatics, polars/resins, and asphalthenes. The

branched chain and straight alkanes and cycloalkanes are the saturates. The aromatic fraction is made of mono- or polycyclic hydrocarbons with alkyl or cycloalkane substitutes. The carbon atoms in aromatics form a circle and where we have six carbon atoms forming the circle, it gives rise to the benzene ring. They have sweet aroma and hence the name. The asphalthenes and resins are non-volatile, containing atoms other than carbon and hydrogen such as sulphur, nitrogen, and oxygen but differs in their size and solubility [12, 16]. Crude oil can also be fractionated into three classes based on the aliquots used. The successful aliquots used are hexane, benzene and methanol. These aliquots are able to successfully elute paraffins, aromatics and asphalthenes, respectively [17]. These bulk fractions are not necessarily petroleum products which result from the refinery process but are used in petroleum laboratory fractionation studies [16].

The paraffins are saturated hydrocarbons with general formula, C_nH_{2n+2} where 'C' and 'H' are carbon and hydrogen, respectively and 'n' stands for the number of the elements they are attached to in the formula. The paraffins can be straight or branched chain. Paraffins are in gaseous state at room temperature when the number of C atoms are less than 5, those between 5 and 15 are liquid and those above 15 are solids [18, 19].

2.1.1 IMPACT OF OIL SPILL ON THE ENVIRONMENT

Millions of gallons of oil are spilled all over the world yearly [13, 20]. By definition oil spill is a distinct incident in which there is a discharge of oil either by accident, through neglect or with intent over a relatively short time [1, 21]. Prospecting and drilling of crude oil in the marine environment, from a defective oil extractor or a problem with a super tanker which is caused by a fire outbreak are some of the causes of oil spills [22]. The spill of these oils form slick which has increased surface area and brings disastrous consequences to the marine environments. A slick is shown in Figure 2.2.

When the slicks are formed on the sea or water surfaces, aquatic life is rudely interfered with, that may have a corresponding ripple effect on economic activities of oil producing countries [23]. The fishing industries of the oil producing countries are interfered with; fishermen are not able to carry out their fishing activities which consequently lead to job losses. The tourism sector is equally affected because the beaches become inaccessible. Health issues also become rife.

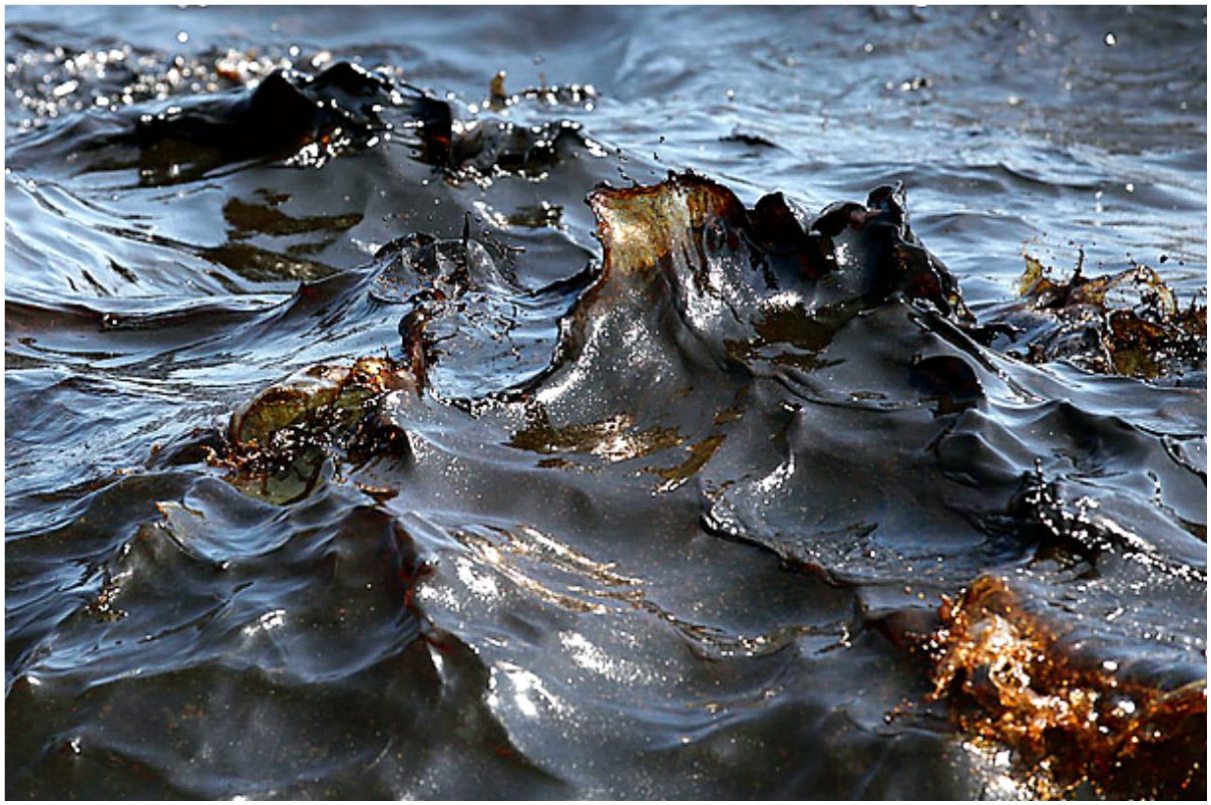

Figure 2. 2 The Slick formation during an oil spill [24].

2.1.2 REMEDIATING MEASURES FOR DEALING WITH OIL SPILL

There are generally five ways that are currently employed in dealing with oil spill. They include;

1. Leaving the oils to degrade naturally. This can be done if there is no possibility of it affecting the aquatic environment or getting to the shore line. However, it has been found that not all the components of the crude oil degrade [25].
2. The use of booms to contain the spill and collecting it with skimmer equipments from the surface of the water [26].
3. In situ burning which is normally used when everything else fails involves the burning of the oil spilled on the sea or water surfaces. This method though promising with a yield of about 95 % efficiency can cause serious challenges to the environment. The burning causes air pollution and the heat generated can be destructive to aquatic life by destroying both fish and plant life in the marine environment [27].
4. The application of chemicals called dispersants to breakdown the oil and hasten its biodegradation. The chemicals are made up of surfactants which are partly soluble in oil and in water. Due to the amphiphilic nature of the surfactant, the dispersants are able to minimise the surface tension between the oil and the water. Upon application of external energy, the oil slicks are broken down into small droplets. Application of the chemical dispersant allows for remediating greater quantities of the oil spill within a short period of time. The above notwithstanding, the toxicity levels are high and it is expensive [28].
5. Finally, the use of biological agents to hasten the degradation of the oil. This process is usually slow and makes use of fertilizing agent like nitrogen and phosphorus to speed the process. In view of this, its effectiveness depends on whether the fertilizer used is water soluble [25, 28].

2.1.3 ANALYSES OF CRUDE OIL

Crude oil is made up of different components. These include the paraffins, aromatics and asphalthenes. These bulk components are classified based on their molecular weight and the aliquots used in their elution. To separate crude oil into its bulk fractions, there exists chromatographic methods such as open-column liquid chromatography (OCLC) used to separate a single compound from a mixture and the use of high performance liquid chromatography (HPLC) in the separation, identification, and quantification of each component in a sample. HPLC uses pumps to transport a liquid under pressure containing the sample mixture through a column filled with a solid adsorbent material. The components in the sample then combines individually and uniquely with the adsorbent material, making them discharge and separate at contrasting rates as they come out of the column. Size exclusion chromatography (SEC) is a technique whereby the particles in a sample solution are isolated by their size, and molecular weight, and thin-layer chromatography (TLC) which can be used for separating a mixture into its component parts. Again TLC can be used to test for the presence of various materials, to monitor the rate and advancement of a reaction or to find the purity of a product [16, 29].

This research focuses on the use of open-column liquid chromatography to fractionate crude oil into some bulk fractions because it is appropriate and recommended for crude oil laboratory analyses. This method of chromatography when employed for laboratory crude oil analyses mostly uses silica gel as the stationary phase and crude oil as the mobile phase. Asphaltenes are insoluble in n-pentane, n-hexane- or n-heptane, which implies that, depending on the n-alkane used, the asphaltenes will not dissolve. The saturates or paraffins are generally eluted with n-hexane, polar compounds with acetone-toluene, and the aromatics with toluene. With the help of rotary evaporator (Figure 2.4), the eluates are evaporated from the separated fractions under mild vacuum [16, 29].

Using the open column chromatography (Figure 2.3), crude oil can be fractionated into three classes based on the aliquots used. The successful aliquots are the hexane, benzene, and a mixture of benzene and methanol which are able to elute the paraffins, aromatics and the asphaltenes [17].

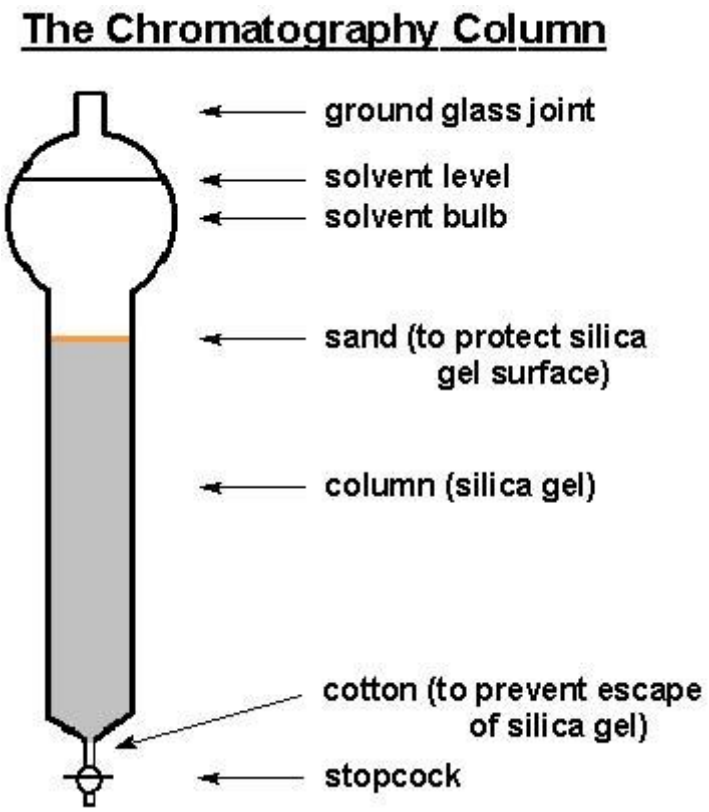

Figure 2. 3 Diagram of Chromatography column used for open-column liquid chromatography [30].

Figure 2. 4 Rotary Evaporator Used In Concentrating The Separated Crude Oil Fractions [31].

The gas chromatography-mass spectrometry (GC/MS) device is used for the analysis of crude oil and its bulk fractions, that is to classify and specify the components of the crude oil and the concentrated fractions [25, 29].

The mass spectrometer (MS) of the GC/MS has the potential to confirm and identify compounds separated by the gas chromatography (GC) through the retention time associated with a spectral pattern. It works by using the intensities of one to three selected ions and comparing it to the intensity of a special target ion with the same spectrum. The ratios of the samples are compared to the ratios of a standard and when the sample ratios lie in the standardised range and the confinement time also matching that of the standard, it is considered present [16].

2.2 PHOTOXIDATION

Photooxidation occurs by way of light-catalysed reactions that oxidize and reduce the carbon in hydrocarbons contained in petroleum. These light-catalysed reactions or photoreactions

can happen either directly or indirectly. The direct photoreactions occur when the reactant or substance involved absorbs light energy to form less stable transition; and indirect photoreactions happen when other chemical species in solution absorb light energy. The most important factors for photooxidation are the intensity of radiation and chromophores which are known to be light absorbing [13].

Crude oil spilled in the marine environment forms slicks. These slicks formed undergo some weathering processes [13]. This weathering process begins immediately when the crude oil is spilled into the sea to change it into different forms which are physically and chemically different from the source crude oil. This process comprises of evaporation, volatilization, emulsification, dissolution and finally oxidation. The oxidation processes may also be chemical, photo induced or microbial [13, 25].

Crude oil as a mixture of complex organic compounds with a greater percentage of it being hydrocarbons can undergo some oxidation reactions to form water and carbon dioxide. The chemical equation describing the process is shown below in equation 2.1;

$$A + O_2 \longrightarrow H_2O + CO_2 \qquad (2.1);$$

A, representing organic compounds [13].

Unlike the parent hydrocarbon, the oxidized hydrocarbon is water soluble. Hydrocarbons are oxidized in the order of small molecules (i.e. up to C20) followed by the larger molecules. The aliphatic n-paraffins (n-alkanes) is initially oxidized within the same molecular weight range, followed by cyclic alkanes (naphthalene) , the polycyclic aliphatic and aromatic hydrocarbons [13]. Aromatic hydrocarbons that are photooxidized results in the formation alcohols, aldehydes, ketones, and acids [25]. Hence, the extent of oxidation can be determined based on the residue, the type and dispensation of the residual compounds [13].

Hydrocarbons are not able to absorb light well so photooxidation involving them happen indirectly. Heterogeneous photooxidation, which involves a liquid-solid and liquid-liquid interface reactions has been found to be important. Heterogeneous photolysis of adsorbed species on natural particulate matter may result from the surface photocatalyst by redox reactions [13].

Photooxidation depends on the following factors;

(1) The electromagnetic spectrum in which the light source lies and it intensity,

(2) The modified optical properties of the surface of the water occasioned by the dissolved particles and the petroleum hydrocarbons,

(3) The optical properties of petroleum hydrocarbons' present,

(4) and photo-quenchers and activator compounds that are present in the water.

This research focuses on catalysing the photooxidation of crude oil using the semiconductors TiO_2 and Fe-TiO_2 photocatalysts.

2.3 SEMICONDUCTOR PHOTOCATALYSTS AND PHOTOCATALYSIS

Semiconductor photocatalysts has over the years generated enormous interest in many researchers with many articles written on this topic. This interest has been so because of the varied applications of semiconductors like ZnO, CuO, TiO_2, $SrTiO_3$, CdS and many more. Amongst the heterogeneous semiconductor photocatalysts TiO_2 enjoys a huge interest base amongst many researchers because of the excellent qualities it possesses in the area of photocatalysis especially in dealing with environmental challenges. It is readily available, less expensive and has a tunable bandgap that can be exploited for more photocatalytic efficiency under sunlight [2].

2.3.1 PHOTOCATALYSIS

Photocatalysis involves a set of reactions that make use of light or photon energy to activate a catalyst to speed up a reaction [32, 33]. The photocatalyst is a solid semiconductor and amongst them TiO_2 is the current choice for many researchers [34]. Photocatalysis has been used in the decomposition of organic substances into harmless or environmentally compatible substances such as water and carbon dioxide [3, 7, 17, 35-41].

The mechanism of TiO_2 photocatalysis is outlined below;

1. TiO_2 has a unique lone pair of electrons in its outer orbital which it makes use of during photocatalysis. When photons from UV and sunlight with energy greater than or equal to the band gap energy of the TiO_2 interacts with its surface, it excites the lone pair of electrons from the valence band (VB) to the conduction band (CB). The photon excited electrons create a hole in the VB and an electron in the CB. This electron-hole pair evokes a set of oxidation and reduction reactions at photo excited surface of the TiO_2 [3, 10, 35, 38]. The above phenomenon just described is diagrammatically presented in Figure 2.5 below.

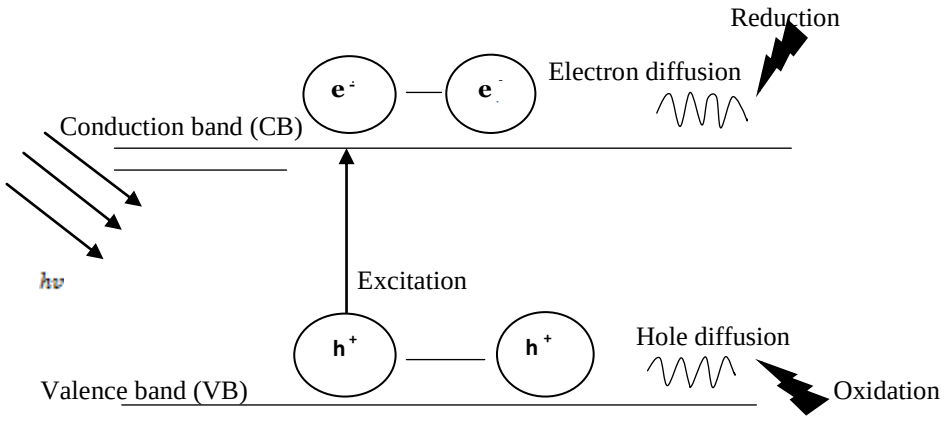

Figure 2. 5 Formation of Photoinduced electron-hole pair. Adopted from reference [42].

2. The electrons and holes created react with dissolved oxygen and water molecules creating reactive oxygen species that react with the adsorbed organic compounds at

the surface of the photocatalyst. The electrons (e^-) that migrates to the CB are strongly reducing and the holes (h^+) at the VB are strongly oxidizing. The organic compounds at the surface of the photoexcited TiO_2 forms intermediates which are further broken down into water and carbon dioxide [3, 43].

3. For efficient TiO_2 photocatalysis, recombination of the photo-excited electron (e^-) and holes (h^+) should be prevented. To achieve this the electron – hole pair gets trapped at the surface which makes recombination impossible for some time. The presence of scavenger electrons prolongs the recombination time and makes photocatalysis possible. The presence of oxygen at the surface serves as the scavenger electrons which also prevent recombination [3, 8, 44].
4. The scavenger oxygen forms superoxide radical ($O_2^{\cdot -}$) which is further protonated to form hydroperoxyl radical ($HO_2^{\cdot}$) and finally H_2O_2. The hydroperoxyl radical formed also serves to prolong recombination of the electron-hole pair. It must be stated that without the presence of water the photocatalysis reaction may not proceed [3].

2.4 PROPERTIES OF TiO_2

Titanium dioxide as an excellent n- type semiconductor has evoked a wide appeal among the semiconductors that are used in photocatalysis application [3, 35]. This photocatalyst material has many useful purposes and the worthy of mention is the attention it has drawn in environmental purification. It is superb when it comes to its ability to degrade organic compounds [7]. One important property that gives it the environmental appeal is its availability. It has been available since its discovery in 1923. It exists in eleven phases out of which three are common. They are the anatase, brookite and rutile phases [7, 45, 46]. The crystal structures of these three phases have been provided in Figure 2.6 below.

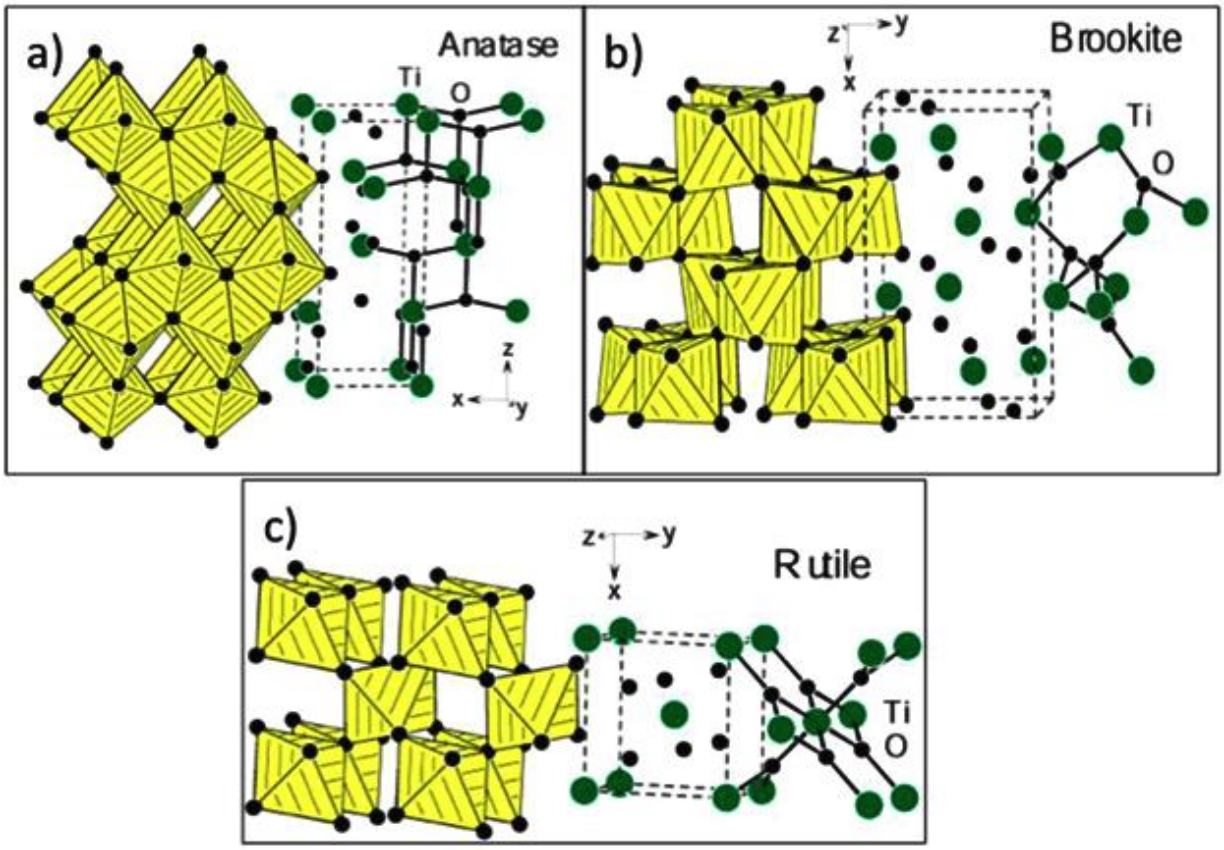

Figure 2.6 The Three Common Crystal Structures Of TiO_2 [43.]

Other properties that place TiO_2 ahead of the other semiconductors are; it strong stability in the presence of aqueous electrolyte solutions, it is relatively low in cost, it has high refractive index and is able to adsorb organic substances at its surface and absorb UV radiation. In addition to the foregoing it is non-toxic, has long time corrosion resistance, outstanding incident photoelectric conversion coherence and dielectric constant, photostability and favourable thermal stability [3, 5, 7-11, 35, 47, 48].

For photocatalytic applications the anatase phase is the preferred choice. This is because; it gives the peak quantum yields obtainable from TiO_2. It is thermodynamically stable and forms at lower temperatures of below 600 ^{o}C. Also it has a higher surface area, high density and most active sites for photocatalysis [6, 49].

In spite of the excellent photocatalytic ability of TiO_2 it has some drawbacks that affect its potential to effectively harvest much of the sunlight energy because it absorbs in the UV radiation [10, 11, 35, 48]. The UV component of solar light is 5 % corresponding to a wavelength of 300-400 nm [7, 10, 11, 35, 48]. This is so because, it has a large bandgap energy of 3.0 eV for rutile and 3.2 eV for anatase phases of TiO_2 corresponding to $\lambda < 390$ nm and its photon absorption relies to a large extent on their bandgap energy. These photons can only be absorbed by the photocatalyst if the photon energies are higher than or equal to that of the TiO_2 bandgap energy [10, 35]. The afore mentioned challenges can be resolved by modifying the TiO_2 in order to reduce its bandgap energy to that in the visible light region corresponding to 400 - 700 nm.

2.5.0 DOPING TITANIUM DIOXIDE

To be able to extend the TiO_2's ability to utilize sunlight energy and widen its applications the band gap energy ought to be engineered to make the TiO_2 visible light active. Doping the TiO_2 with a metal or non-metal has been found to help in this direction. This doping which is done with a foreign ion has been found to enhance the visible light absorption capabilities of the TiO_2 photocatalyst [10, 11, 35, 47, 48]. A number of non-metals like N, S, C, B, and F, have been doped into TiO_2 successfully. Amongst the non-metals N has been deemed the best bet for doping TiO_2 to narrow the band gap energy [10, 11]. Also metals like V, Zn, Eu, Ti, and Fe have been successfully doped into TiO_2 and this narrowed the band gap with Fe-doped TiO_2 being the most excellent [10, 47, 50]. The dopants when added to the TiO_2 brings on board extra energy levels to the band structure, which are able to trap photo induced electrons or holes to prevent recombination which allows them to successfully migrate to the surface. Increasing the impurity ion or dopant concentration or the oxygen defects causes a red shift of the absorption edge. This enhances the optical properties of the TiO_2 to enable it utilize the sunlight energy and promotes [7, 10, 47].

It is well established that Fermi level (the highest energy state electrons occupy in a material at absolute zero temperature) is very close to the CB tail at a high oxygen vacancy concentration. Owing to this, the higher oxygen vacancies can bring about enhanced absorption of photon energy below the direct bandgap. Again, the metal induced gap (midgap) states below the CB edge turn to broaden as the oxygen vacancy concentration increases. The band of defect states which comes from oxygen vacancies is close to the CB edge and gives way for photoexcited electrons to be easily exchange between the two bands. These are the electrons from the VB which move to an oxygen vacancy level when excited by a photon from visible light. When this happens, the electrons move from both VB and oxygen vacancy level localized states to the tailed CB thereby improving their optical properties [10].

2.5.1 NON-METAL DOPING

Non-metal dopants can also enhance the photocatalytic ability of TiO_2. Non-metals such as N, B, F, C and Cl have high ionization energies and high electronegativity and when incorporated into the structure of the TiO_2 is able to narrow the band gap and shift the absorption edge so that it is able to utilize the sunlight energy.

The non-metal dopants affect the VB by interacting with the oxygen 2p electrons. The localized states or p states of non-metallic dopants generally form the impurity levels and lie above VB, and in effect widen the optical absorption edge of TiO_2. Non-metal dopants within the surface can exist as isolated atoms rather than clusters and distribute the dopant states above the VB maximum, thereby enhancing its ability to harvest sunlight [10].

Nitrogen (N) element has been proven to be excellent among the non-metals for doping TiO_2 to enhance its visible light responsiveness [51]. The nitrogen is incorporated through oxygen substitution and this narrows the bandgap due to the mixing of the nitrogen 2p and oxygen 2p states [10]. The nitrogen for the doping is provided by a urea source.

2.5.2 METAL DOPING

To successfully dope TiO_2 with a metal and obtain favourable homogeneity, sintering must be done at high temperature to bring about particle agglomeration. The metal dopant makes available more trapping sites for electrons and holes in contrast to non-metal dopants. Again, electron trapping happens rapidly compared to hole trapping [10].

The surface properties of TiO_2 intrinsically could be altered by the preparation method, process, and doping. These methods of preparation determine the surface separation and transfer of charge carriers by producing surface states where electrons and holes are spatially trapped and moved for subsequent redox reactions [10].

The substitution of metal ions can introduce an intraband state which is close to CB edge. This brings about a red shift in bandgap adsorption due to sub-bandgap energies.

This notwithstanding, the diffusion of metal atoms is hard to achieve in solid materials under low temperature conditions. This results in inhomogeneous distributions of dopants and limited depth near a subsurface region [10, 52].

Fe-doped TiO_2 presents itself as an excellent candidate for photocatalysis owing to the fact that it has a uniquely semi-filled electronic configuration and its identical ionic radius to Ti^{+4} which makes it easy for it to be added to the crystal structure of TiO_2 [53]. The Fe^{+3}doped into TiO_2 lower the recombination of the excited electrons and the holes when it interacts with light and so bringing about an improvement in its photocatalytic activities [54].

The challenge with metal doping is thermal instability, which makes TiO_2 difficult to reuse as a photocatalyst [10].

2.6.0 SYNTHESIS OF TiO_2 AND MODIFIED TiO_2

Several processes have been employed over the years to synthesize TiO_2. They are the liquid process (sol–gel, solvothermal, hydrothermal) and solid state processing routes (mechanical

alloying/milling, mechanochemical, radiofrequency (RF) thermal plasma and other routes such as laser ablation [55].

It is a well-known fact that the preparation TiO_2 influences its properties which are dependent on the size, morphology and crystalline phase of the prepared TiO_2. These have the potential to affect the performance of the TiO_2 photocatalyst [56].

From the above methods, the sol–gel and the hydrothermal methods are the most common and widely used for the synthesis of TiO_2 for photocatalytic applications. This is because it is easy to prepare in the lab and the processing method is also economical.

2.6.1 SOL GEL METHOD.

Sol gel method is one of the commonest methods used for the preparation of TiO_2 powder. Uncontrolled conditions of the prepared powders by the sol–gel method have mostly resulted in TiO_2 that lacked the properties of uniform size, shape, and unagglomerated state [55].

To achieve results that favour the properties of TiO_2, controlled process conditions are very important [45, 55]. The following are some of the parameters;

(a) The precursor's concentration of titanium alkoxide [46, 55].

(b) The water-titanium molar ratio which affects the size, stability, and morphology of the produced sol from the alkoxides. This is because the colloidal TiO_2 formed at a high ratio produces the small size of the particles formed.

(c) The processing temperature, peptization process and the peptization agents.

(d) The pH of the prepared solution which significantly affects the final size of TiO_2 powder [45, 55].

2.6.2 HYDROTHERMAL SYNTHESIS OF TiO_2.

Hydrothermal synthesis is widely used especially for the production of TiO_2 photocatalyst. Hydrothermal synthesis is usually carried out in a steel pressure vessel known as autoclave with or without Teflon liners. It is done under carefully controlled conditions of temperature or pressure with the reaction in an aqueous solution. The temperature can be set in such a way to rise above the boiling point of water and as a result reach the pressure of vapour saturation. This makes it possible to increase the crystallinity of the TiO_2 nanoparticles by converting the amorphous TiO_2 into crystalline [50, 57].

Hydrothermal synthesis has the following advantages:

(a) The reaction conditions are easy to carry out in a straight forward manner.

(b) It is environmentally friendly and low in energy consumption.

(c) The temperature for crystallization is below 200 °C [57].

Generally, most syntheses of pure TiO_2 and its modified forms have been obtained by post - heat treatment of the sol-gel/hydrothermally prepared amorphous TiO_2 especially with nitrogen dopants at high temperature into the TiO_2 lattice. This notwithstanding, calcining the sol-gel/hydrothermally prepared amorphous TiO_2 under high temperature may cause agglomeration and abnormal growth of crystals which gives it a small surface area and reduces the number of photoactive sites[48]. An alternative is to use mild conditions. This is done by drying the sample after hydrothermal treatment at a lower temperature (of about 70^oC) for some time (for 24 hours or more). These mild conditions are not easy to achieve with nitrogen doping of TiO_2. However some successes have been achieved according to prior works [48, 58, 59].

The incidence of oil spills coupled with their devastating effect on the environment, the remediation measures currently in use, and intense research activities ongoing to provide

more efficient remediation measures have been reviewed. The research is to assess the remediation effects of pure and modified TiO_2 photocatalyst on the photodegradation of crude oil in spill environments. Attention will be directed towards the synthesis and characterization of pure and modified TiO_2, determination and analyses of the components of the crude oil and conducting photodegradation tests on the fractions of the crude oil using the pristine and modified TiO_2 photocatalysts.

The intermediate photoproducts formed will be identified through GC/MS. The extent of degradation of the various crude oil fractions will be compared.

CHAPTER THREE

3.0 MATERIALS AND EXPERIMENTAL PROCEDURES

3.1 INTRODUCTION

This chapter presents the materials used in this project and a detailed description of the experimental procedures and methods.

3.2 MATERIALS AND EQUIPMENT

The following reagents were used and were of analytical grade. No further purification was adopted in the various processes. Rhodamine Blue dye, Isopropanol (IPA), titanium tetraisopropoxide (TTIP), Dichloromethane (DCM), Benzene, Hexane, Acetone and the Methanol were purchased from Sigma Aldrich, U.S.A., Ethanol was purchased from Fisher Scientific, U.K., Hydrochloric acid (HCl) from Analar, England and Crude oil was obtained from Tullow Oil Ghana.

3.3 EQUIPMENTS USED IN THE STUDY.

The following are the tools and equipment used during this project. Some of the equipment were used in sample preparation and others where used in the characterization of the prepared samples. They are X-ray Diffractometer, UV-Vis spectrophotometer, Gas Chromatography/ Mass Spectrometer, Fourier-Transform Infrared Spectroscopy (FTIR) Spectrometer, Scanning Electron Microscope with Energy Dispersive X-ray Spectroscopy, Thermogravimetric Analyser, and Differential Scanning Calorimeter.

3.4.0 SYNTHESIS OF TiO2 NANOPARTICLES

Mild hydrothermal synthesis was used in the synthesis of the TiO_2 nanoparticles using metal alkoxide precursors. In a typical synthesis of TiO_2 nanoparticles, TTIP and isopropanol were mixed in the ratio 1:10 v/v and named solution A. Solution B which is made up of hydrochloric acid (HCl) and water (H_2O) in a 1:10 v/v ratio was also prepared. Solutions A

and B were added together and subjected to rigorous stirring at 1200 rpm for 24 hours to form a milky solution. This was done at room temperature to promote homogeneity and stability of the solution.

The resultant mixture was then centrifuged at 1800 rpm for 15 minutes and washed several times with distilled water. The solid particles collected after centrifugation were dispersed in a solution made up of 60 ml of water and 60 ml of ethanol and autoclaved at 115 ℃ for 8 hours. The autoclaved particles were dried in an oven at 70 ℃ for 48 hours. The as-prepared powder was then crushed and sieved with 75 µm sieve to obtain the TiO_2 particles. The as-prepared TiO_2 particles and the flow diagram for the entire synthesis process is presented in Figures 3.1 and 3.2, respectively.

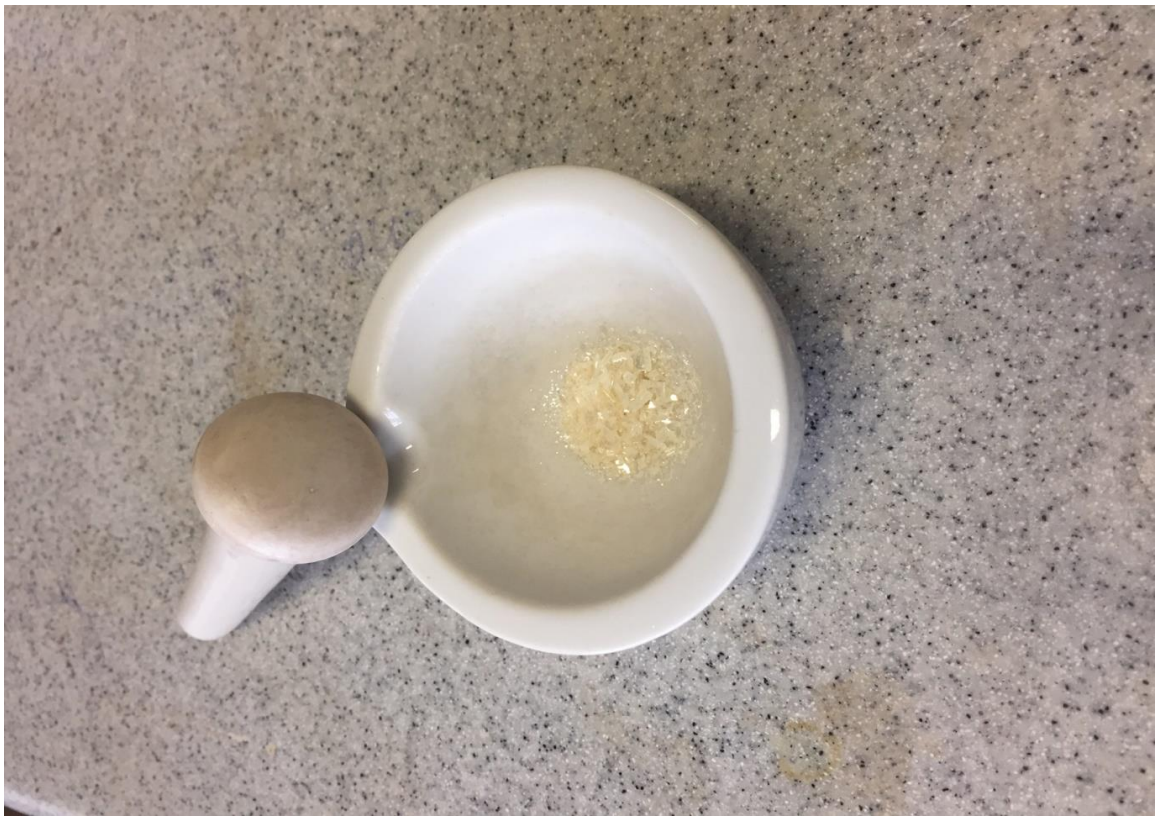

Figure 3. 1 A picture of TiO_2 crystals.

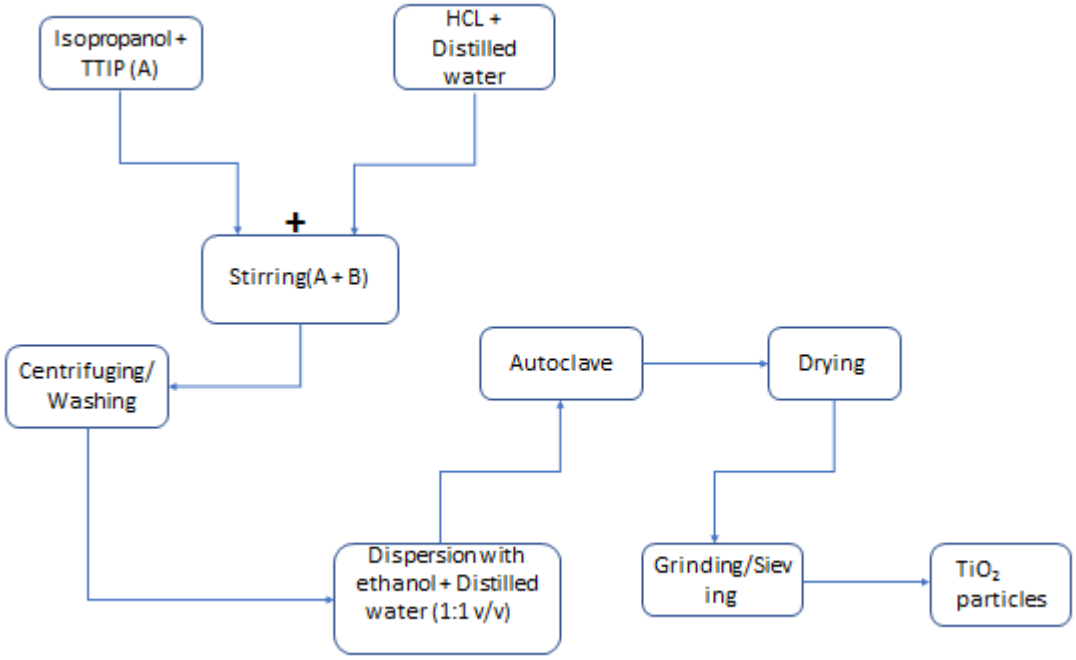

Figure 3. 2 Flow diagram of the mild hydrothermal synthesis of pure TiO_2.

3.4.1 MILD HYDROTHERMAL SYNTHESIS OF IRON DOPED TiO_2

The method used for the synthesis of iron doped TiO_2 is similar to that used for the synthesis of TiO_2. The doping was done by adding 88 mg of $FeCl_3.6H_2O$ to the resultant solutions of A and B and subjected to rigorous stirring at 1200 rpm for 24 hours to allow the formation of light brown milky solution. This was done at room temperature to promote homogeneity and stability of the milky solution.

The resultant solution was then centrifuged at 1800 rpm for 15 minutes and washed several times to obtain a neutral pH. The particles obtained after centrifugation were dispersed in a solution made up of 60 ml of water and 60 ml of ethanol and autoclaved at 115 ℃ for 8 hours. The autoclaved particles were dried in an oven at 70 ℃ for 48 hours. The as-prepared

powder was then crushed and sieved with 75 µm sieve to obtain the Fe doped TiO_2 particles. The as-prepared Fe-TiO_2 particles can be found in Figure 3.3 below.

Figure 3. 3 A picture of Fe-TiO_2 crystals.

3.5.0 CHARACTERIZATION OF THE TiO_2 AND Fe-TiO_2.

The as-produced TiO_2 and Fe-TiO_2 particles were characterized to investigate their structure and properties using X-ray diffraction(XRD), scanning electron microscopy (SEM), energy dispersive X-ray spectroscopy (EDX) and Fourier-transform infra-red (FTIR) spectroscopy. The other techniques include diffuse reflectance spectroscopy (DRS), thermogravimetric analysis (TGA), differential scanning calorimetry (DSC) and UV-Vis.

3.5.1 X-RAY DIFFRACTION (XRD) ANALYSIS OF Fe-TiO2 AND TiO_2 SAMPLES

X-ray powder diffraction (XRD) is a rapid analytical technique basically used for phase identification of a crystalline material and also makes information available on unit cell dimensions.

The phases present and the microstructure of the TiO_2 and Fe-TiO_2 particles was identified using X-ray powder diffraction (XRD) patterns and were obtained using Bruker D8 theta with anode material = Cu K-Alpha1 [Å]: (1.54060) and generator settings (40 mA, 45 kV). The XRD patterns of all the randomly oriented powder specimens were recorded in the 20°-70° 2θ range with a step size of 0.017°.

The Debye Sherer's equation was used to compute the crystallite sizes of the TiO_2 and the Fe-TiO_2. A picture of the XRD used is shown in Figure 3.4 below.

Figure 3. 4 A picture of XRD.

3.5.2 SCANNING ELECTRON MICROSCOPY (SEM)

The scanning electron microscope (SEM) makes use of a focused beam of high-energy electrons to produce a variety of signals at the surface of solid samples. These signals that are produced from electron-sample interactions gives information about the sample including external morphology (texture), chemical composition, and crystalline structure and orientation of materials making up the sample [60]. The SEM analysis was done using FEI Nova NanoSEM 450 fitted with EDX acquisition detector.

3.5.3 ENERGY DISPERSIVE X-RAY (EDX)/ENERGY DISPERSIVE SPECTROSCOPY (EDS)

The energy dispersive x-ray spectrometer operates on the basis of the detection of characteristic X- rays emitted when a high energy electron beam interacts with an element. These X-rays are those produced from the de-excitation of electrons and holes created by the materials interaction with high energy beams. Since electron energy levels are quantized and unique for every element or material, the detected emitted characteristic X-ray energies is used to identify the elements. The EDX analysis was done using FEI Nova NanoSEM 450 fitted with EDX acquisition detector.

3.5.4 FOURIER TRANSFORM INFRARED (FTIR)

The Vertex 70v (Bruker) was used to record the transmission FTIR spectra. The range used was 4000-400 cm^{-1} with 4 cm^{-1} resolution. The FTIR spectrometer consists of a source, interferometer, sample compartment, detector, amplifier, A/D convertor, and a computer. The source produced the radiation which interacts with the sample through the interferometer to reach the detector. The signal produced is amplified by an amplifier and converted to digital signal by an analog-to-digital converter. Finally, the signal is transferred to a computer in

which Fourier transform is carried out [61-64]. The spectra were recorded and analysed using the Opus software. A picture of the FTIR equipment is shown in Figure 3.5 below.

Figure 3.5 A picture of FTIR.

3.5.5 UV-VIS SPECTROSCOPY

The UV-Vis spectrophotometer or the ultraviolet visible spectrophotometer is used to determine the optical properties of samples, substances or materials within the ultraviolet and visible wavelength ranges (190 to 1100 nm). By the UV-Vis spectrophotometer one can ascertain the amount of light of a particular wavelength that is transmitted or absorbed by a sample, substance or material. The information gathered can be used to determine concentration, structure and the molecular identity of the material.

The UV-Vis of the TiO2 and the Fe-TiO2 was done by adding 20mg of the sample to 40mls of distilled water and the absorbances were taken. The control solution or the blank was distilled water.

On the other hand, 0.1 ml of the mixture of the separated photodegraded crude oil fraction and dichloromethane (DCM) was further diluted with 10 ml of dichloromethane to make it less concentrated for the UV-Vis analysis. In doing the analysis dichloromethane (DCM) was used as the control solution or the blank. A picture of the UV-Vis spectrophotometer is shown in Figure 3.6 below.

Figure 3.6 A picture of UV-Vis Spectrophotometer.

3.5.6 DIFFUSE REFLECTANCE SPECTROSCOPY (DRS)

DRS was carried out using an Ocean Optics USB-4000 spectrometer with a dedicate reflectance probe. Illumination was supplied by a Halogen/Deuterium source across the UV-Vis range. Powders were compressed into a flat film between soda lime glass microscope slides prior to measurement and a commercial polytetrafluoroethylene (PTFE) reflectance standard was used as a reflectance calibration. The Kubelka Munk function [65, 66] was then used to compute the optical band gap the TiO_2 and the Fe-TiO_2.

3.5.7 THERMOGRAVIMETRIC ANALYSIS (TGA) / DIFFERENTIAL SCANNING CALORIMETRY ANALYSIS (DSC)

The thermal analysis of the TiO_2 and the Fe-TiO_2 was done using the TGA and DSC. The TGA was used to analysis the mass change of the material as a function of temperature. Whiles the DSC was used to measure the quantity of energy absorbed (endothermic) or released (exothermic) between the sample and a reference material. The mass of the sample used was 20 mg and the temperature range was 25 °C – 750 °C at a heating rate of 10°C /min.

3.6 FRACTIONATING THE CRUDE OIL SAMPLE

The crude oil was separated into three classes (Figures 3.4 and 3.5). This was achieved by adding 50 ml of crude oil to 181 g silica gel in a chromatographic column. 500 ml of n – hexane was first added to the crude oil in the column to elute the paraffins. Secondly, 500 ml of Benzene was also added to the residual crude in the column for the elution of the aromatics. Lastly, a solution of 250 ml of Methanol and 250 ml of Benzene was again added to the residual crude after the second elution, to elute the asphaltenes.

The eluate samples of paraffins, aromatics and the asphalthenes concentrates were formed by evaporating the solvent-crude oil fractions mixture using the rotary evaporator at 40 °C. The pictures and flow diagram of the fractionating process are shown in Figures 3.7 and 3.8, respectively.

Figure 3. 7 A picture of the setup used in separating the various fractions of the crude oil.

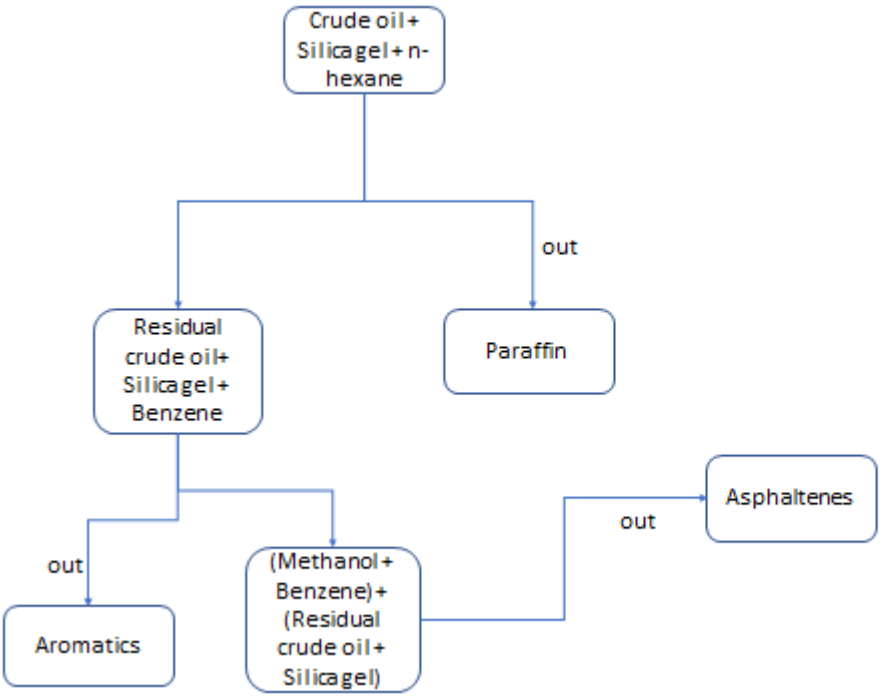

Figure 3. 8 Flow diagram of the separation of the Crude oil using open column liquid chromatography.

3.7 PHOTODEGRADATION OF THE CRUDE OIL FRACTIONS

0.2 ml of the crude oil fraction was measured and added to 50 ml of distilled water in a 200 ml beaker. 50 mg of the photocatalyst was added to the mixture of the crude oil fraction and the distilled water.

The resultant mixture was placed in the light source chamber that is the UV or visible light chamber. In the case of using sunlight, the crude oil-water-photocatalyst mixture was placed in the sun. Continuous stirring at 350 rpm was done to ensure that the photocatalyst mixes well with the water and crude oil. Irradiation was done continuously for four hours after which 7 ml of dichloromethane was added to the resultant mixture to dissolve the degraded crude oil. The dichloromethane with the dissolved degraded crude oil (or crude oil fraction) was separated from the photocatalyst and water using separation funnel. The dissolved oil is further centrifuged at 600 rpm for 15 minutes to ensure that all residual photocatalyst are

separated. The dichloromethane with the dissolved crude oil or fractions was characterized. Pictures of the photodegradation of the fractions of crude oil under sunlight and UV irradiation are shown in Figure 3.9.

Figure 3. 9 Pictures of the Photodegradation of the crude oil fractions under (A) sunlight and (B) UV irradiation.

3.8 GAS CHROMATOGRAPHY MASS SPECTROMETRY (GC/MS)

These are two processes that have been combined for effective chemical analysis. The GC is able to separate the sample into components whilst the MS is used to identify substances especially in petroleum products. The two together when used in identifying substances help to make conclusive identification [67]. The GC component used for the analyses was PerkinElmer Clarus 580 and the MS was PerkinElmer Clarus SQ 8S.

These were the GC/MS conditions employed; Oven: Initial temp 80 °C for 0 min, ramp 10 °C/min to 240 °C, hold 2 min, ramp 5 °C/min to 280 °C, hold 10 min, Injection temperature of 250°C, injected volume = 1 µL, Split = 20:1, Carrier Gas = He, Solvent Delay = 2.50 min, Transfer Temp = 250°C, Source Temp = 150°C, Scan: 50 to 500Da, Column dimension 27.0 m x 250 µm.

CHAPTER FOUR

4.0 RESULT AND DISCUSSION

4.1 INTRODUCTION

This chapter presents the results and discussion of the synthesis and characterisation of TiO_2 and Fe-TiO_2, fractionation of the crude oil and its analysis and the photodegradation of the crude oil fractions using the as-prepared TiO_2 and Fe- TiO_2.

4.2 CHARACTERIZATION OF TiO_2 and Fe- TiO_2

4.2.1 XRD PLOTS of TiO_2 and Fe- TiO_2

Figure 4.1 below shows XRD patterns of pure TiO_2 and Fe-doped TiO_2 powders. It is observed that the XRD peaks confirm the formation of TiO_2 and Fe-TiO_2. The intensity of the Fe-doped TiO_2 peaks is slightly weaker than that of the pure TiO_2. The peaks for the Fe-TiO_2 also shifted slightly to higher 2 theta values. These observations can be attributed to the presence of the Fe^{3+} in the structure of the TiO_2.

From the XRD spectrum of TiO_2 and Fe-TiO_2 in Figure 4.1, the anatase phase was the only observed phase and its peaks (101), (004), (200), (105) and (204) were quite wide and not sharp. This is indicative of incomplete crystallization due it amorphous component [43, 68, 69]. The amorphous phase present in the anatase phase of the TiO_2 plays an important role in the photocatalytic process [70].

The anatase phase of TiO_2 is admitted to be the best active phase for degradation of organic materials. This is because it is formed at lower temperatures which make it crystallite sizes smaller than that of the rutile which is formed at higher temperatures (>500 ^oC), this gives the anatase phase high surface area. A large surface area enables the anatase phase to adsorb more of the organic materials for photocatalysis [3]. Due to the fact the photocatalytic activity is dependent on the active sites which is also influenced by the crystallite size, the

Debye-Scherer equation (equation 4.1) was used to compute the crystallite sizes of the Fe-doped TiO_2 and pure TiO_2.;

$$d = \frac{\kappa\lambda}{\beta\cos\theta} \qquad (4.1)$$

Where:

D is the mean size of the of the crystallites, K is the shape factor and a good approximation is 0.9, λ is the X-ray wavelength, β is the full width at half maximum (FWHM) in radians of the X-ray diffraction peak and θ is the Braggs angle (deg.) [43, 71].

Table 4. 1 Crystallite sizes of the TiO_2 and the Fe-TiO_2.

Sample	**Peak Position 2θ(°)**	**FWHM 2θ(°)**	**Crystallite Size (nm)**
TiO_2	25.32109	2.07748	4.10
Fe-TiO_2	25.3054	2.0863	3.85

From the Table 4.1 above it can be seen that the crystallite size of the Fe-TiO_2 is smaller than that of the TiO_2. This is so because the successful addition of the Fe^{3+} did not allow the growth of the TiO_2 crystallite [72-74].

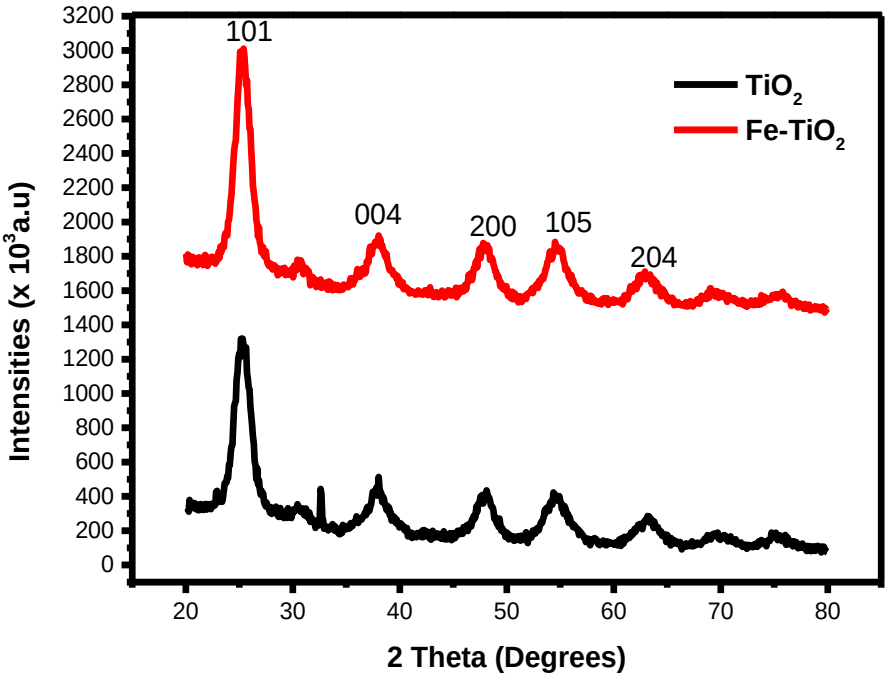

Figure 4. 1 XRD patterns of the Undoped and Fe-doped TiO_2 powders.

4.2.2.0 OPTICAL PROPERTIES ANALYSIS OF TiO_2 AND Fe-TiO_2.

4.2.2.1 UV-VIS SPECTROSCOPY

The optical properties of the TiO_2 and Fe-TiO_2 were determined using the Ultraviolet-visible (UV-vis) spectroscopy and the Diffuse Reflectance Spectroscopy (DRS). The results for the UV-Vis and DRS analyses are presented in Figures 4.2 and 4.3, respectively.

The Figure 4.2 below illustrates the UV-Vis spectra of the as-prepared TiO_2 and the Fe-TiO_2. It can be seen that TiO_2 absorbs photons in the UV range (300 – 400 nm) but not in the visible range (> 400 nm). On the hand the Fe-TiO_2 curve shows a red shift into the visible region which shows it absorbs beyond the 400 nm and hence active in the visible light.

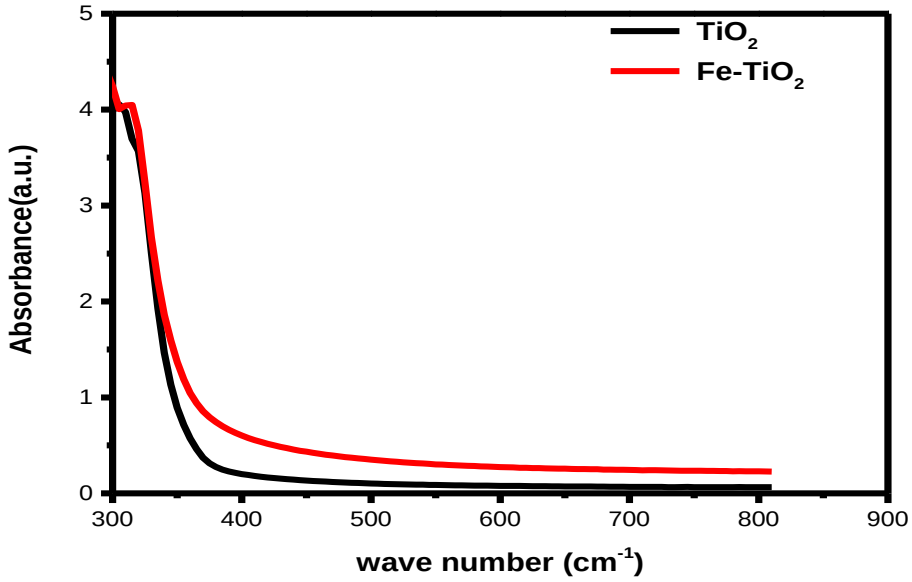

Figure 4. 2 The UV-VIS spectroscopy of TiO_2 and Fe-TiO_2

4.2.2.2 DIFFUSE REFLECTANCE SPECTROSCOPY (DRS)

Figure 4.3 below shows the DRS curves for the as-prepared TiO_2 and Fe-TiO_2. The reflectance of the TiO_2 shows 100 % in the range of 330 – 800 nm which was much higher than that of the Fe-TiO_2 which is about 60 % in the range of about 380 – 800 nm. This means that the TiO_2 is better at reflecting light in the visible range than the Fe-TiO_2. On the other hand it also shows that Fe-TiO_2 absorbed more in the visible light region than that of the TiO_2. This is because a higher reflectance means a lower absorption and the vice versa. This therefore suggests that the Fe-TiO_2 photocatalyst will be more active in the visible light region than the TiO_2. This agrees with published works[75]

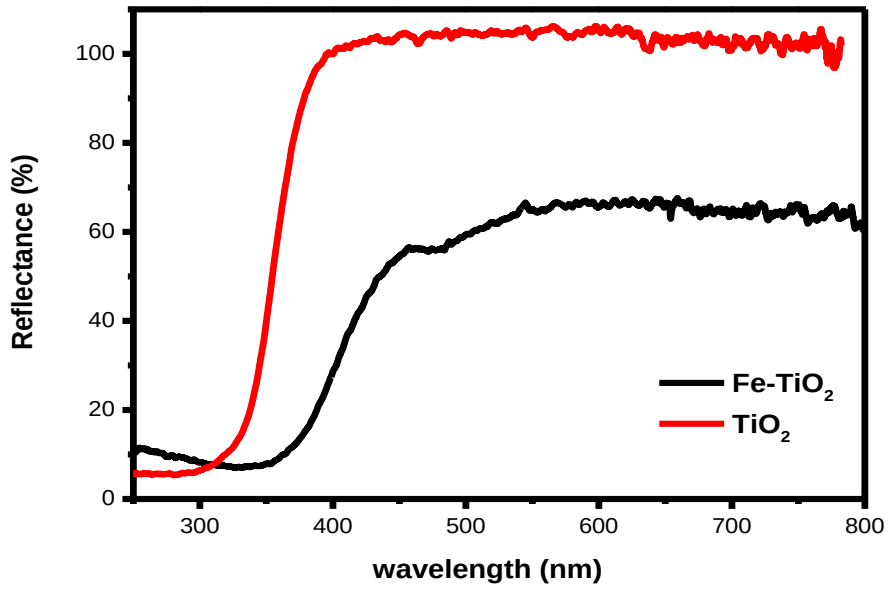

Figure 4. 3 Diffuse Reflectance Spectroscopy (DRS) of the as-prepared TiO_2 and Fe-TiO_2

4.2.2.3 DETERMINATION OF THE OPTICAL BAND GAP

Figure 4.4 shows the optical band gap of TiO_2 and Fe-TiO_2 from the Kubelka Munk transformed reflectance [65, 66]. Comparing the estimated band gaps of Fe-TiO_2 and TiO_2 from Figure 4.3 it can be observed that there is a reduction in the band gap energy from 3.12 eV for the TiO_2 to 2.9 eV for the Fe-TiO_2 (Table 4.2). This reduction in the band gap is as a result of the Fe^{3+} dopant in the TiO_2 structure which the XRD (Figure 4.1) and EDX (Figure 4.5b) confirms. The decrease in band gap agrees with published works[76]

.

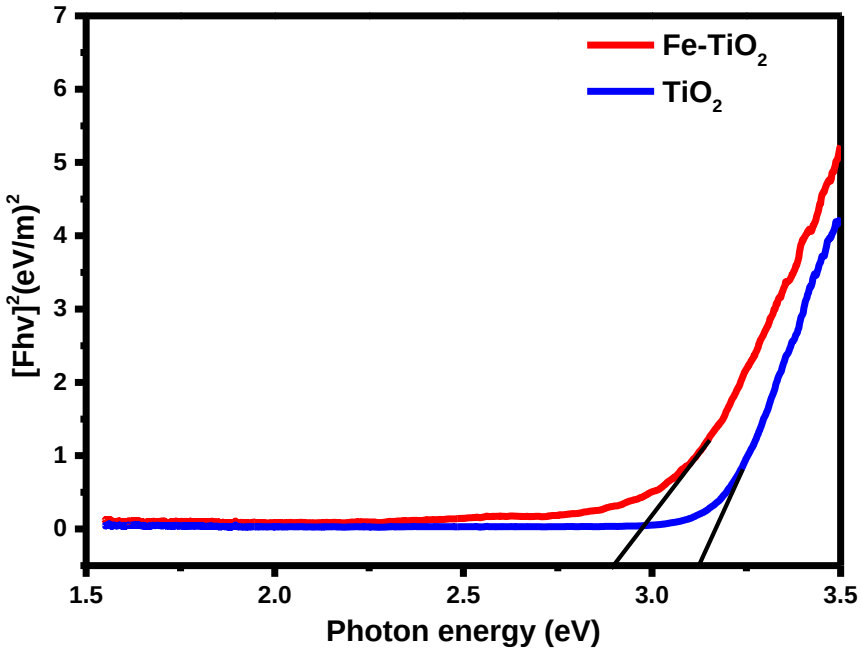

Figure 4. 4 Kubelka Munk transformed reflectance for estimating the optical band-gap energy of TiO_2 and Fe-TiO_2.

Table 4. 2 Values of the estimated band gap of TiO_2 and Fe-TiO_2

Photocatalyst	Estimated band gap
TiO_2	3.12 eV
Fe-TiO_2	2.9 eV

4.2.3 MORPHOLOGICAL AND SURFACE ANALYSIS OF THE TiO_2 AND Fe-TiO_2

4.2.3.1 ENERGY DISPERSIVE X-RAY SPECTROSCOPY (EDX)

The elemental composition of the TiO_2 and Fe-TiO_2 was analysed with EDX. Figure 4.5 shows the energy dispersive X-Rays spectroscopy (EDX) of TiO_2 (Fig. 4.5a) and that of Fe-TiO_2 [Fig. 4.5b]. Figure 4.5a shows peaks for Titanium and Oxygen suggesting the formation of pure TiO_2 without any impurities which agrees with the XRD results. Table 4.3 shows the weight % and atomic mass % also confirming the formation of TiO_2.

Figure 4.5b and Table 4.4 also shows peaks for Fe, Ti and O which also suggests the TiO_2 was successfully doped with the Fe^{3+} without any impurities forming. This also agrees with the XRD results. The unidentified peaks at 2 Kev can be attributed to the Pt that was used for sputter coating the samples before the analyses.

Table 4. 3 Elemental Analysis of The As- Prepared TiO_2.

Element	Weight %	Atomic %
Titanium	53.91	28.11
Oxygen	46.09	71.89

Table 4. 4 Elemental Analysis of The Fe-TiO_2.

Element	Weight %	Atomic%
Titanium	62.96	36.74
Oxygen	35.90	62.70
Iron(III)	1.13	0.57

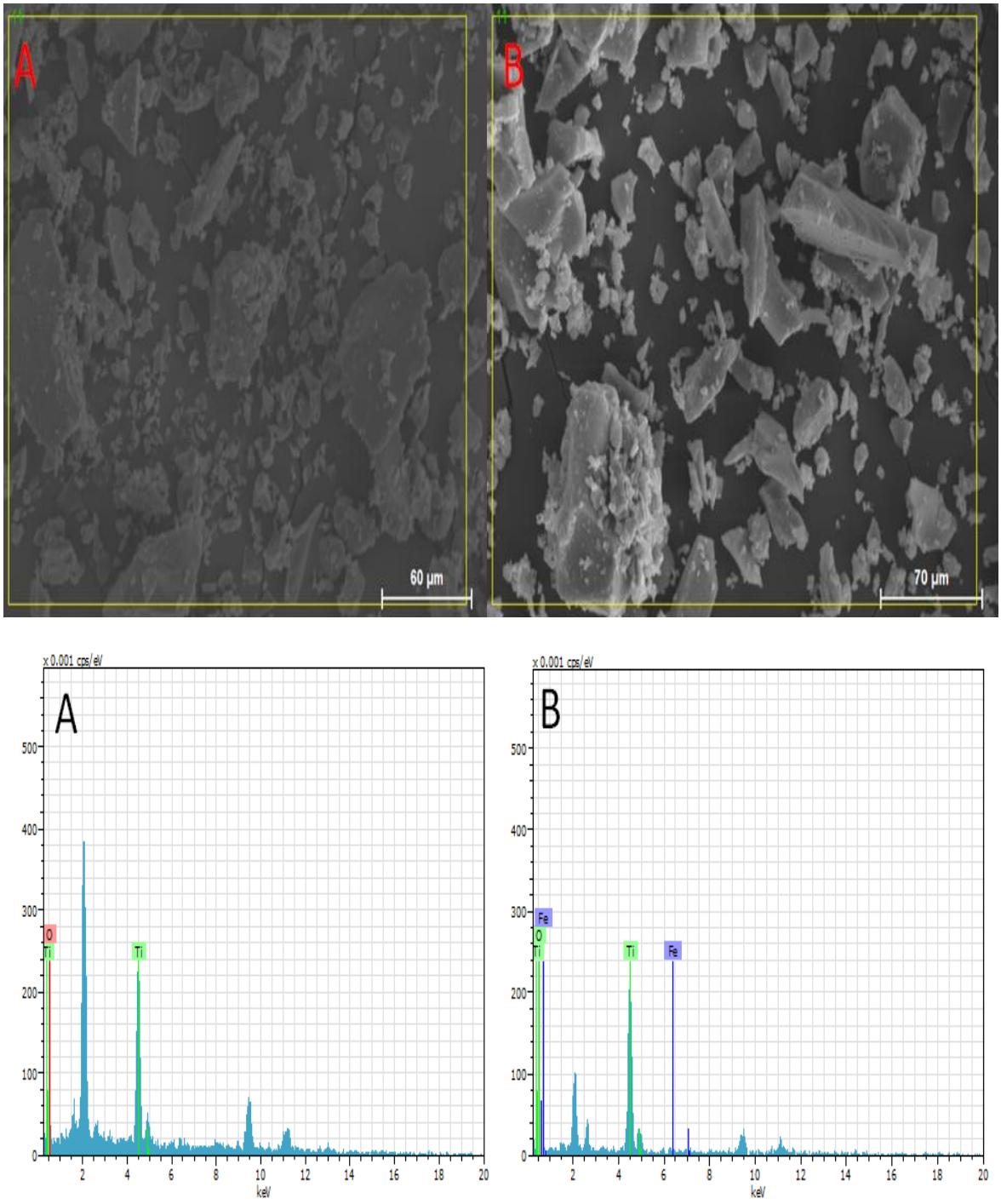

Figure 4. 5 Energy Dispersive X-ray Spectroscopy (EDX) of (A) TiO_2 and (B) Fe-TiO_2, respectively.

4.2.3.2 SCANNING ELECTRON MICROSCOPE (SEM)

The Figures (4.6a and 4.6b) below show the Scanning Electron Microscope (SEM) images of

Fe-TiO_2 and TiO_2, respectively. It shows the surface morphology of the TiO_2 and Fe-TiO_2.

From the images it is observed that the sizes are not uniform (smaller particles can be seen on the larger particles) and they appear in chunks and this is due to the grinding of the samples.

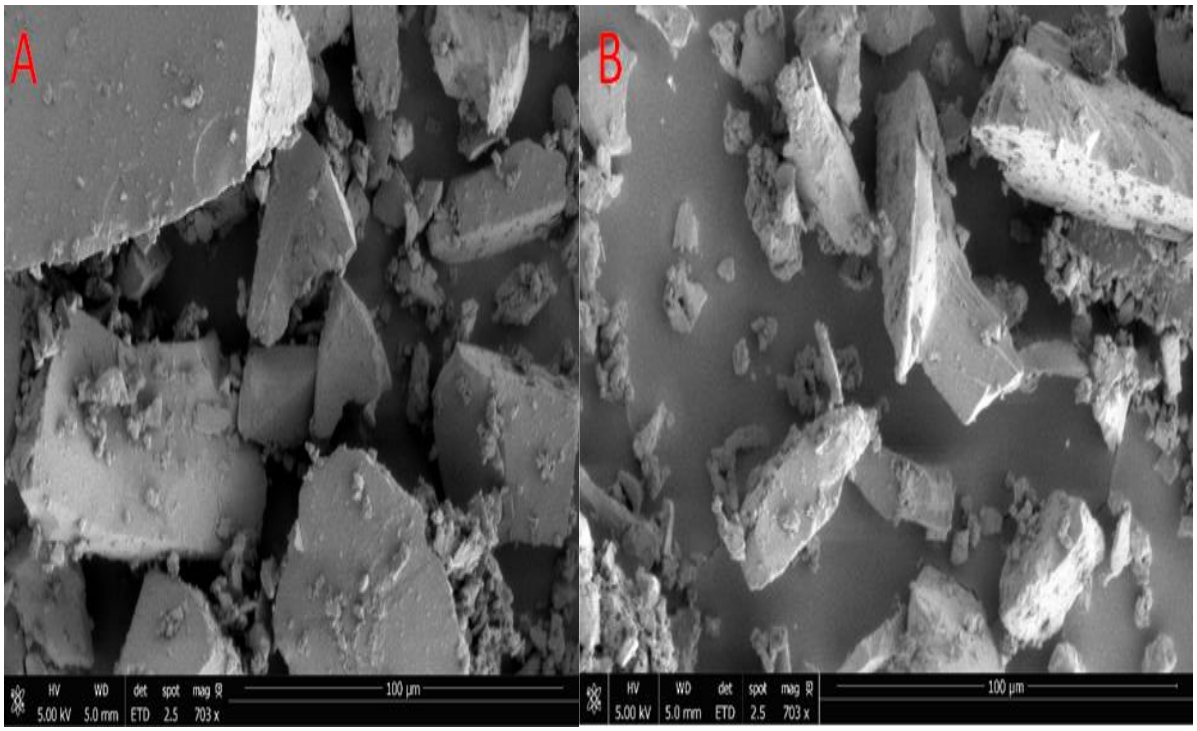

Figure 4. 6 Energy Dispersive X-ray Spectroscopy (EDX) of (A)TiO_2 and (B)Fe-TiO_2, respectively.

4.2.4 THERMAL ANALYSIS OF THE AS-PREPARED TIO_2 AND FE-TIO_2

The thermal behaviour of the TiO_2 and the Fe-TiO_2 using DSC and TGA were conducted from room temperature to 750 ℃ to examine their thermal behaviour as shown in Figures 4.7 and 4.8. Generally the thermal behaviour of TiO_2 depends on the chemical composition, preparation condition, and phases that are present [77, 78].

4.2.4.1 DIFFERENTIAL SCANNING-CALORIMETRY (DSC)

Figure 4.7 shows the DSC of the as-prepared TiO_2 and the Fe-TiO_2. It can be observed that they both follow similar pattern and possess similar features. The first peak which is endothermic at 95°C for TiO_2 and 110°C for the Fe-TiO_2 represents the loss of adsorbed water on the surface corresponding to a mass loss as revealed in Figure 4.8. The second peak observed at a temperature 350 °C for TiO_2 and 400 °C for Fe-TiO_2 is exothermic represents

the oxidation and decomposition of the organic substances present. This also resulted in a mass loss as can be seen in Figure 4.8. Phase transformation from anatase to the rutile phase occurred above 400 °C [78, 79].

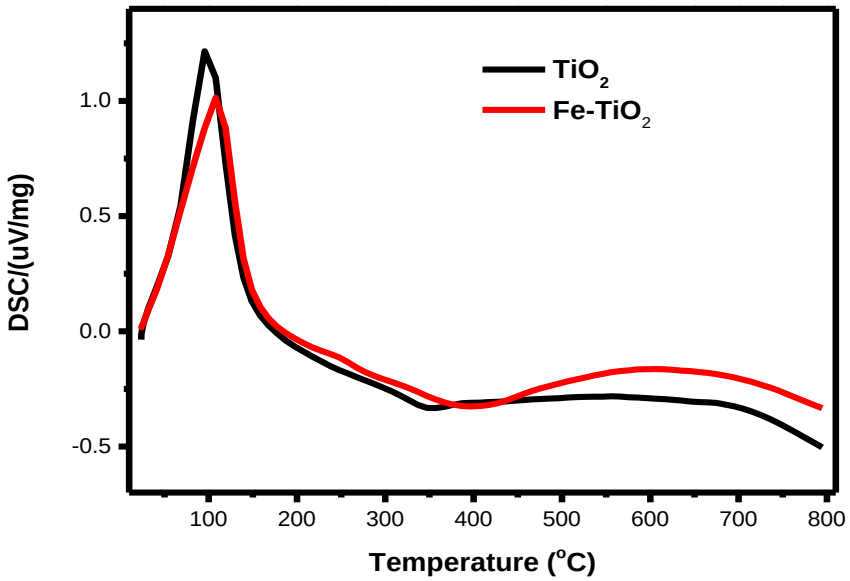

Figure 4. 7 Differential Scanning-Calorimetry (DSC) of the as-prepared TiO_2 and Fe-TiO_2

4.2.4.2 THERMOGRAVIMETRIC ANALYSES (TGA)

Figure 4.8 is the TGA results of the as-prepared TiO_2 and Fe-TiO_2. Three stages of transitions are observed from the curve in both samples. Considering the TiO_2 curve, the first stage is showing a 14 % mass loss due to the elimination of the ethanol and alcohol present in the sample when the temperature increase from 25 ^{o}C to 140 ^{o}C. The second stage also shows another 7 % of mass loss attributable to the complete decomposition of the organic compounds in the sample as the temperature increased from 140 ^{o}C to 443 ^{o}C. Taking note of the Fe-TiO_2 curve, the first stage shows a 14 % loss in mass which indicates the elimination of the presence of the ethanol and water present in the sample. The second stage also shows another mass loss of 17 % representing the decomposition of all the organic compounds as the temperature increased from 140 ^{o}C to 443 ^{o}C. In the final stage there is no mass loss at

temperatures > 443 ^{o}C. The TGA curve for both samples showed no mass loss after 443 $^{\circ}$C suggesting a total decomposition of all organic components in the TiO_2 [43, 80]. These observations were corroborated with the XRD and FTIR results in Figures 4.1 and 4.4, respectively.

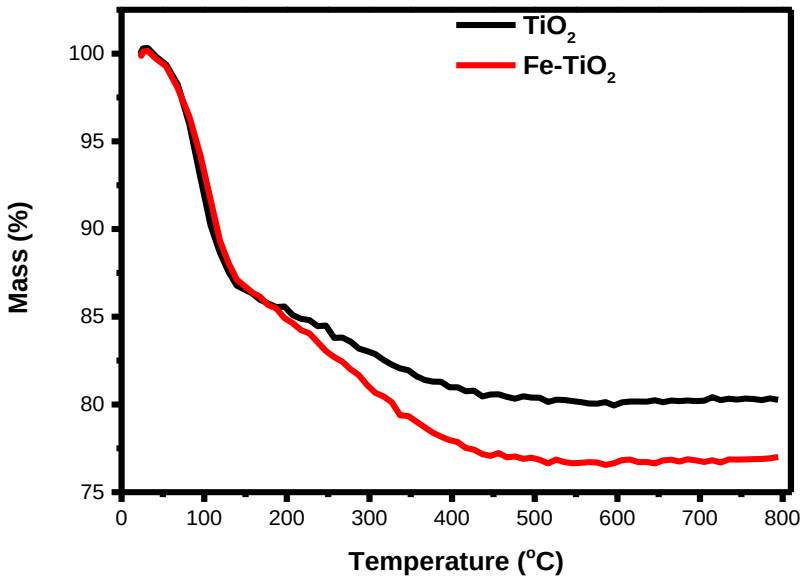

Figure 4. 8 Thermogravimetric Analyses (TGA) of the as-prepared TiO_2 and Fe-TiO_2

4.2.5 FOURIER TRANSFORM INFRARED (FTIR) SPECTROSCOPY ANALYSIS

Figure 4.9 shows that in both the TiO_2 and the Fe-TiO_2 the stretching of the hydroxyl (O-H) bonds occurred between the wave numbers 3000 to 3500 cm^{-1} band. This represents the presence of moisture in the as-prepared samples. Peaks were observed between 1250 to 1750 cm^{-1} band which indicates the stretching of titanium carboxilate that emanated from the TTIP and ethanol as precursors. The peak between 800 to 450 cm^{-1} shows the TiO_2 particles that were formed [81, 82].

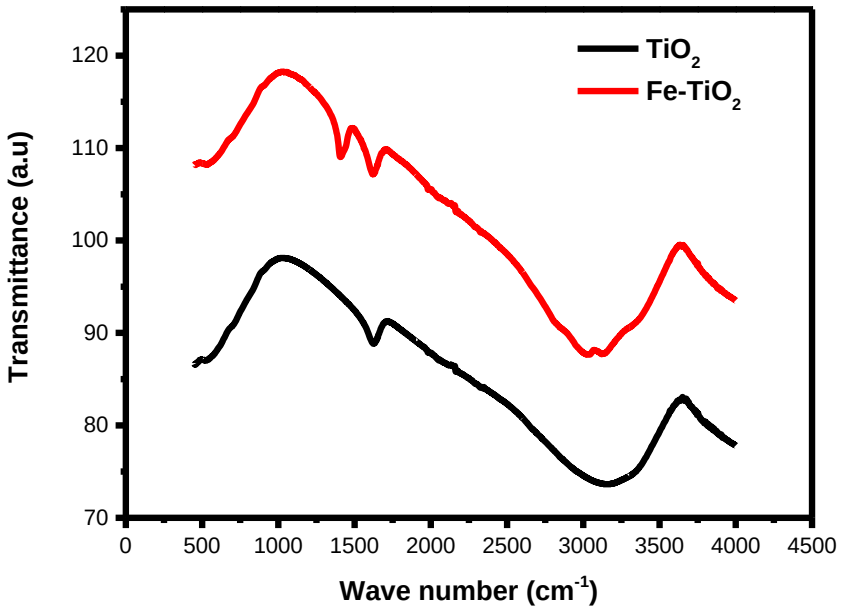

Figure 4. 9 FTIR of TiO_2 and Fe-TiO_2 powders

4.3 FTIR CHARACTERIZATION OF THE FRACTIONS OF THE CRUDE OIL

The separated crude oil fractions; aromatics, asphaltenes and the paraffins were identified using the FTIR going by Abdulkadir et al., 2016 who suggested FTIR as a rapid and cost effective way of analysing crude oil [83]. Akmaz et al, 2011 also used FTIR among other analysis to characterize crude oil [84].

The FTIR showed bands around 2,900 cm^{-1} , 2,850 cm^{-1} , 1500 cm^{-1} and 1350Cm^{-1} due to CH_2 and CH_3 groups [84]. Again absorption bands were identified at 1600 cm^{-1} due to C=C, 1700 cm^{-1} due to C=O, 675cm^{-1}, 700cm^{-1} and 900 cm^{-1} depicting aromatic rings [83]. The identified absorption bands of the crude oil fractions in Figure 4.10 have similar features with the FTIR spectra of crude oil fractions reported by Akmaz et al, (2011), Ali et al. (1989), Peralta-Martinez et al. (2008), Aske et al. (2001), and Buenrostro-Gonzalez (2001) [22, 84-87].

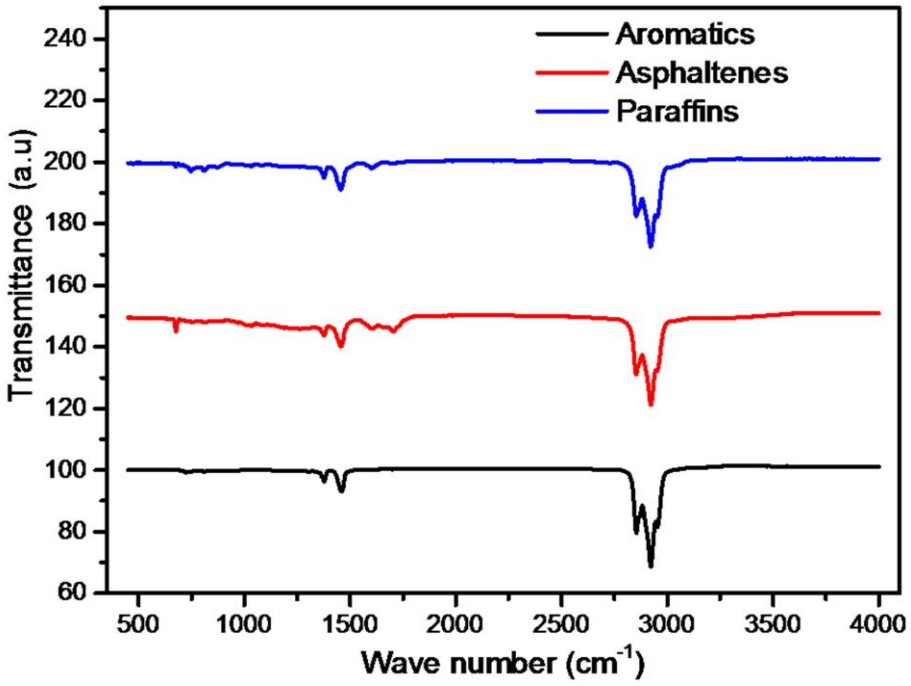

Figure 4. 10 FTIR analysis of the crude oil fractions.

4.4 PHOTOCATALYTIC ACTIVITY OF THE AS-PREPARED TiO_2 AND Fe-TiO_2 ON CRUDE OIL BULK FRACTIONS

The activity of the as-prepared TiO_2 and Fe-TiO_2 on the degradation of the bulk fractions of the crude oil was carried out. Samples were exposed under sunlight, visible light and UV light irradiation for four (4) hours.

4.4.1 UV-VIS OF THE CRUDE EXTRACTS

Characterizing the crude oil bulk fractions by UV-vis spectroscopy is not easy to achieve due to its dark colour even though it is simple, practical and cost effective. The difficulty is curtailed by diluting the crude fractions and their degraded portions in appropriate solvents. The solvent used in diluting them was dichloromethane. The plots below show absorbance against wavelength of the degraded crude oil samples.

It was observed that a general trend emerged from the UV-Vis spectra analysis of the photodegraded crude oil fractions [Figures 4.11a-4.11d; Figure 4.11e- 4.11i (Appendix 1)]. It could be observed that the Fe-TiO_2 was more efficient in the sunlight and visible light

irradiation [Figures 4.11a- 4.11c] and hastened the degradation of the crude oil fractions. On the other hand the TiO_2 with a bandgap of 3.12eV was more efficient in degrading the crude oil fractions under UV light irradiation than the Fe-TiO_2 with a band gap of 2.90eV [Figure 4.11d; Figures 4.11e & 4.11i (Appendix 1)]. Where the TiO_2 was redundant especially in the visible light [Figure 4.11d; Figures 4.11f & 4.11h (Appendix 1)] it was seen to be impeding the light penetration and so derailing the degradation of the crude oil fractions in the solution [41]. It also emerged that photodegradation occurred even without the presence of a photocatalyst; however, the presence of the photocatalyst hastened the photodegradation process. This can be seen in Figures 4.11a-4.11d; Figure 4.11e- 4.11i (Appendix 1) where the Nil+ crude oil fractions showed lower absorbance than the undegraded crude fractions. In the visible light the heat produced contributed to the photodegradation process [85].

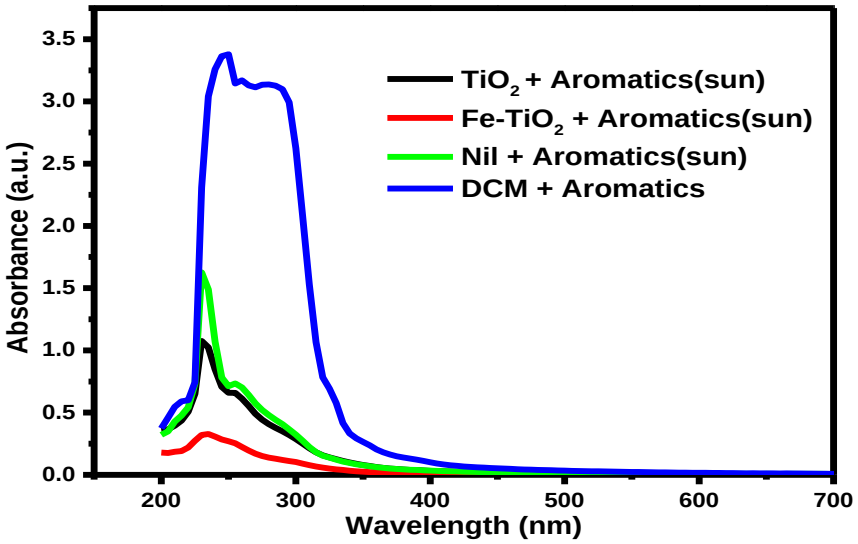

Figure 4. 11a The UV-Vis spectra of the photodegraded aromatics after four (4) hours of sun irradiation with Fe-TiO_2 photocatalyst [Fe-TiO_2+Aromatics (Sun)], TiO_2 photocatalyst [TiO_2+Aromatics (Sun)], photocatalyst [Nil+Aromatics (Sun)]

** [DCM+Aromatics] is the aromatic crude oil fraction dissolved in dichloromethane (DCM) that has not undergone any degradation.

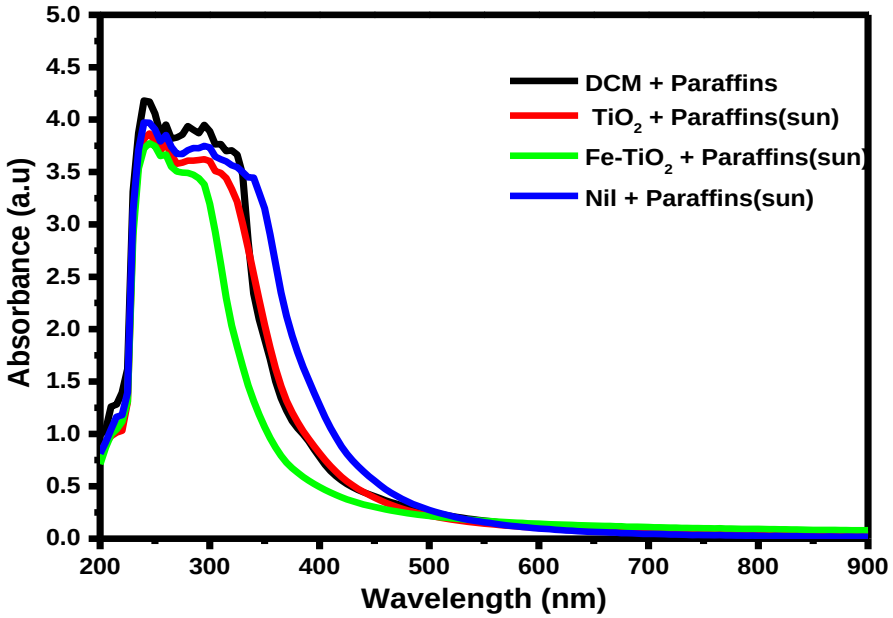

Figure 4.11b The UV-Vis spectra of the photodegraded paraffinic fraction of crude oil after four (4) hours of sun irradiation with Fe-TiO_2 photocatalyst [Fe-TiO_2+ Paraffins (Sun)], TiO_2 photocatalyst [TiO_2+Paraffins (Sun)], no photocatalyst [Nil+Paraffins(Sun)]

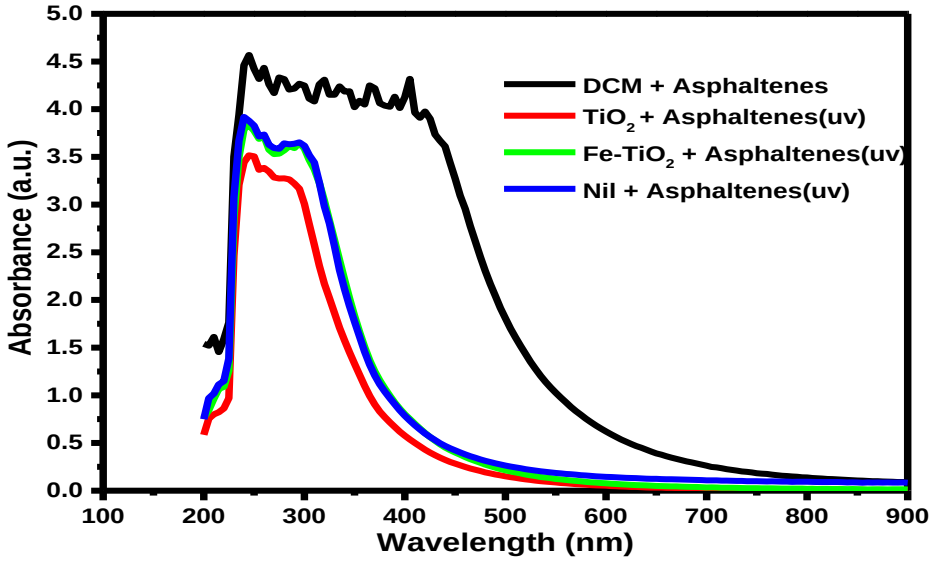

Figure 4.11c The UV-Vis spectra of the photodegraded asphaltenic fraction of crude oil after four (4) hours of UV light irradiation with Fe-TiO_2 photocatalyst [Fe-TiO_2+ asphaltenes (UV)], TiO_2 photocatalyst [TiO_2+asphaltenes (UV)], and no photocatalyst [Nil+ asphaltenes(UV)]

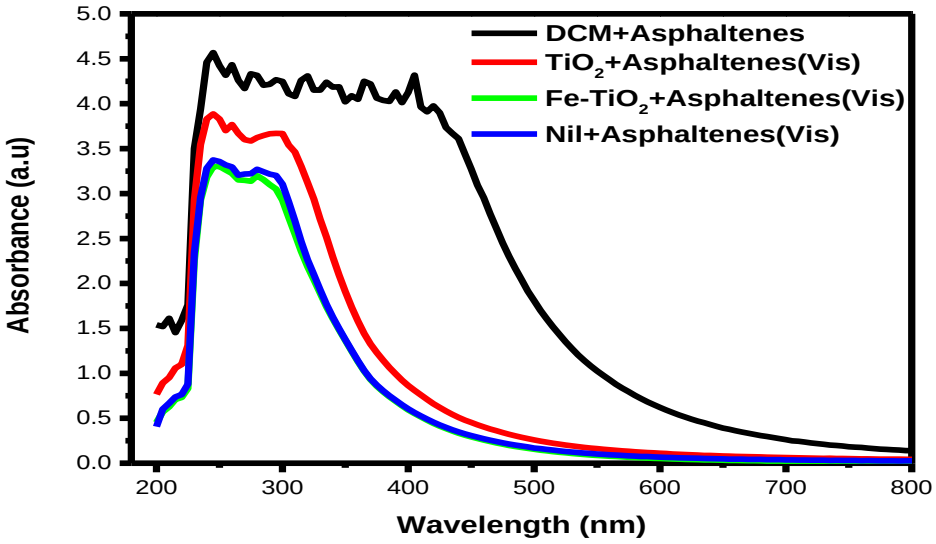

Figure 4.11d The UV-Vis spectra of the photodegraded asphaltenic fraction of crude oil after four (4) hours of visible light irradiation with Fe-TiO_2 photocatalyst [Fe-TiO_2+ Asphaltenes (Vis)], TiO_2 photocatalyst [TiO_2+Asphaltenes(Vis)], no photocatalyst [Nil+Asphaltenes(Vis)]

The extent of photodegradation varied among the crude oil fractions. For instance, under sunlight irradiation, the photodegradation of the aromatic fraction (Figure 4.11a) was more pronounced than the paraffins and the aromatics. This can be attributed to the relatively higher aqueous solubility of the aromatics than the paraffins and asphalthenes. The aqueous solubility enhanced photocatalytic activity due to close proximity of the dissolved aromatics to the hydroxyl radicals generated.

4.4.2 FTIR RESULTS FOR THE PHOTODEGRADED BULK CRUDE OIL FRACTIONS AND THEIR PURE FORMS

The Figures below [4.12a - 4.12d] and in appendix ii [4.12e - 4.12i] show the FTIR results of the photoproducts of the crude oil fractions after subjecting them to four hours sunlight, visible light and UV light irradiation.

Considering all the FTIR results, [Figures 4.12a - 4.12d] and in appendix ii [Figures 4.12e - 4.12i] differences in the spectra of the photodegraded products and the undegraded products

were observed. That is new bands appeared and old bands disappeared. It was observed from the Figures that the undegraded aromatics, paraffins and the asphaltenes [4.12a - 4.12d] and in appendix ii [4.12e - 4.12i] all had bands appearing at around 2,900 cm^{-1} , 2,850 cm^{-1} , 1500 cm^{-1} and 1350 cm^{-1} due to CH_2 and CH_3 groups [84]. Again absorption bands were identified at 1600 cm^{-1} due to C=C, 1700 cm^{-1} due to C=O and 675cm^{-1}, 700cm^{-1} and 900 cm^{-1} depicting aromatic rings [83].

The differences in the spectra between the undegraded crude oil fractions and the degraded fractions in each of the Figures [4.12a - 4.12d] and in appendix ii [4.12e - 4.12i] with or without the photocatalyst can be seen in the bands that appear around 3250 – 3500 cm^{-1} which is indicative of an O-H or an N-H. Bands also appeared around 1700 cm^{-1} and 470 – 800 cm^{-1} which indicates C=O and aromatics, respectively. All these differences are as a result of intermediate compounds forming and some compounds disappearing. These observations confirm that photodegradation took place.

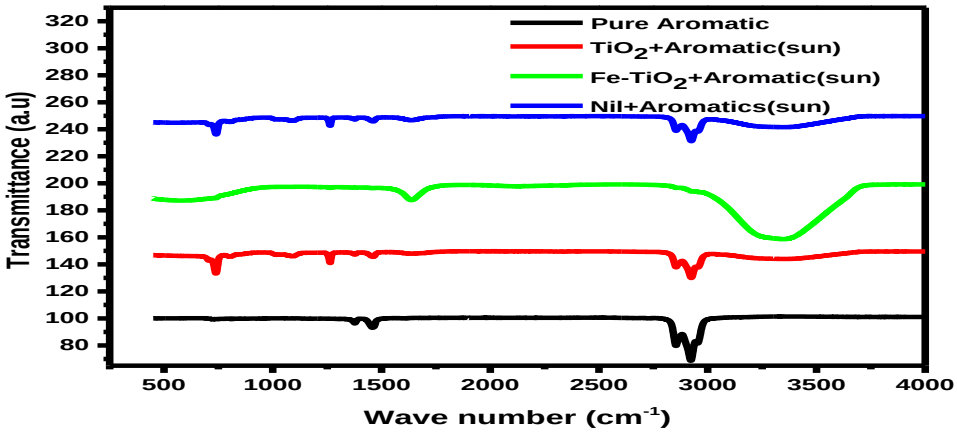

** [Pure Aromatic] is the aromatic fraction that has not undergone any degradation

Figure 4. 12a FTIR peaks of the aromatic fraction of the crude oil which was irradiated under sunlight for four (4) hours using Fe-TiO_2 as photocatalyst [Fe-TiO_2+Aromatic(Sun)],TiO_2 as photocatalyst [TiO_2+Aromatic(Sun)] and without photocatalyst[Nil+Aromatics(Sun)]

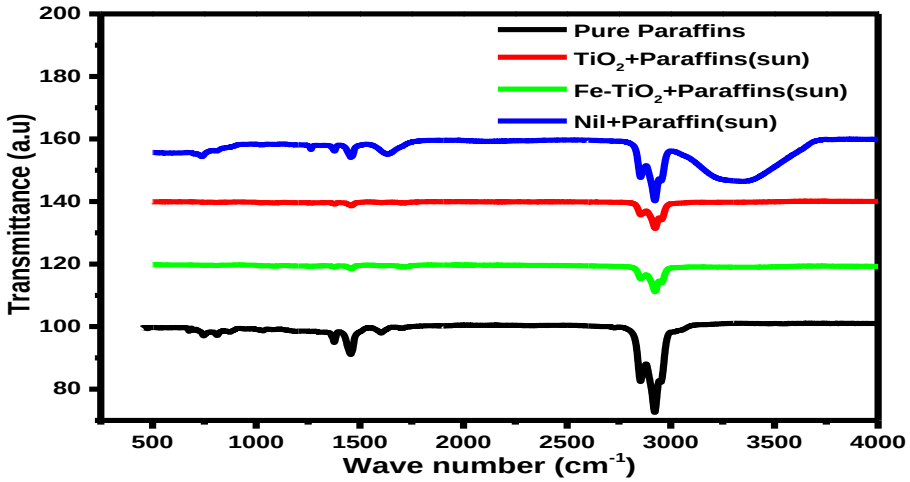

** [Pure Paraffins] is the paraffins fraction that has not undergone any degradation.

Figure 4.12b FTIR peaks of the paraffinic fraction of the crude oil which was irradiated under sunlight for four (4) hours using Fe-TiO_2 as photocatalyst [Fe-TiO_2+Paraffins(Sun)], TiO_2 as photocatalyst [TiO_2+Paraffins(Sun)] and without photocatalyst[Nil+Paraffins(Sun)].

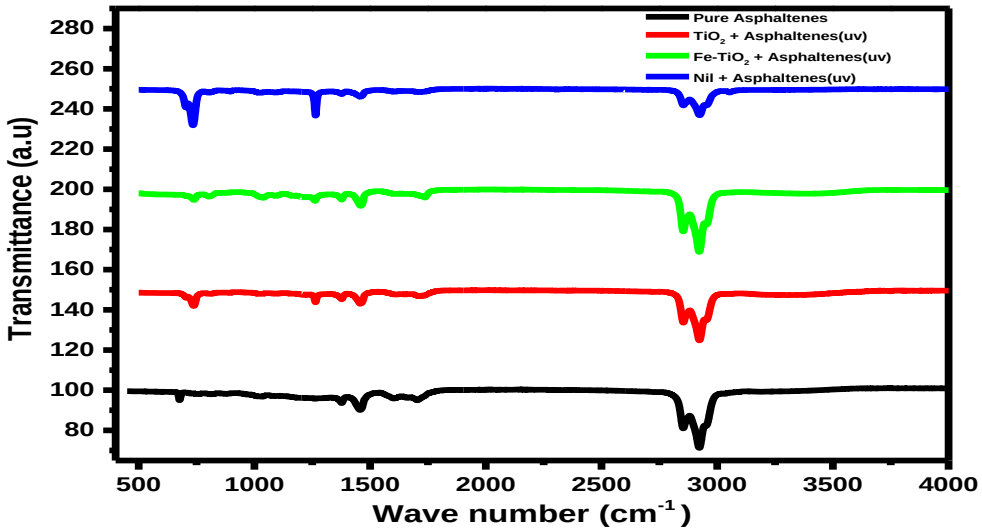

** [Pure Asphaltenes] is the asphaltenic fraction that has not undergone any degradation.

Figure 4.12c FTIR peaks of the asphaltinic fraction of the crude oil which was irradiated under UV light for four (4) hours using Fe-TiO_2 as photocatalyst [Fe-TiO_2+asphaltenes (UV)],TiO_2 as photocatalyst [TiO_2+asphaltenes (UV)] and without photocatalyst[Nil+asphaltenes (UV)]

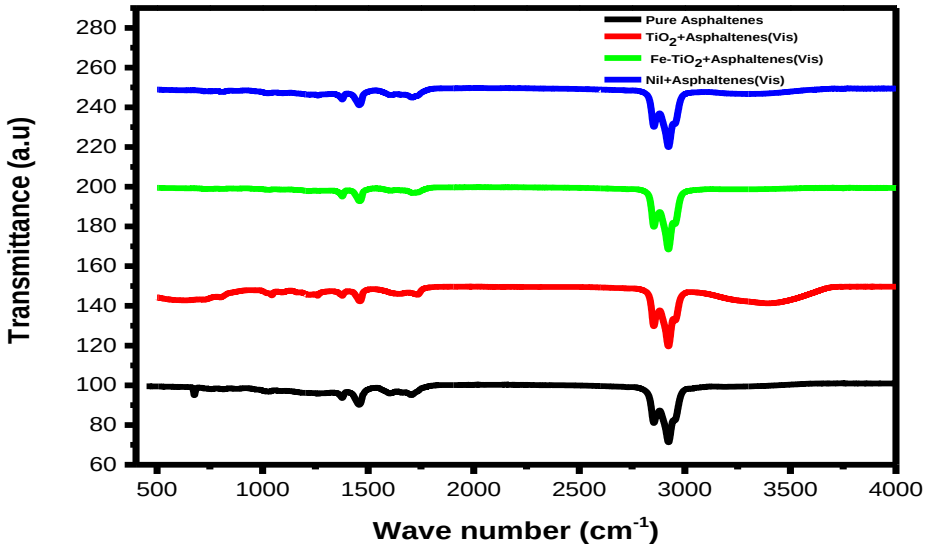

** [Pure Asphaltenes] is the asphaltinic fraction that has not undergone any degradation.

Figure 4.12d FTIR peaks of the asphaltinic fraction of the crude oil which was irradiated under sunlight for four (4) hours using Fe-TiO_2 as photocatalyst [Fe-TiO_2+asphaltenes (Vis)],TiO2 as photocatalyst [TiO_2+asphaltene(Vis)] and without photocatalyst[Nil+asphaltenes (Vis)]

4.4.3 GAS CHROMATOGRAPHY AND MASS SPECTROMETRY (GC/MS)

4.4.3.0 ANALYSES OF THE PHOTOPRODUCTS

The photoproducts from the photodegradation of the crude oil fractions which were irradiated under sunlight for four (4) hours were analysed qualitatively and identified using the GC/MS under the same conditions. The results are presented in Figures 4.13a to 4.13i and in Tables 4.8 to 4.16 in Appendix iii.

4.4.3.1 GC/MS ANALYSIS OF THE AROMATIC PHOTOPRODUCTS

Figures 4.13(a-c) is the GC/MS chromatograms obtained from the photodegradation of the aromatic fraction of the crude oil using TiO_2 and Fe-TiO_2 photocatalysts.

Figures 4.13(b –c) shows that most of the peaks disappeared after photodegradation when compared to the undegraded aromatic fraction in Figure 4.13 (a) and also a hump of

unresolved complex mixtures (UCM) which is evident of severe photodegration of the aromatics [83, 85] were observed. Comparing Figures 4.13(b and c) and Tables 4.9 and 4.10 [in appendix iii], it can be observed that Fe-TiO_2 degraded more of the aromatic fraction of the crude oil, showing more diminished concentration of compounds, disappearance of existing compounds and the appearance of UCM's peaks which indicates severe degradation than the TiO_2+aromatics . This observation is also evident in the FTIR at Figure 4.12a and the UV-Vis spectra at Figure 4.11a.

Formation of unidentified complex mixtures (UCM'S) after the four (4) hour sunlight irradiation is shown in Tables 4.9 and 4.10 in Appendix III. New compounds emerged from the photodegradation of the aromatics as evidenced in Tables 4.5b and 4.5d. There was the disappearance of certain compounds from the aromatics after photodegradation (Table 4.8 in Appendix III) which is presented in Tables 4.5a and 4.5c.

The following compounds were also identified in both Table 4.8 and 4.10 in the Appendix III but were eluted at different retention times; hexadecane, nonadecane, and dodecane 2,6,10 trimethyl which shows they were undegraded or more of it were formed after the four(4) hour sunlight irradiation.

Comparing Tables 4.8 and 4.10 in Appendix III it was observed that tetradecane which was eluted at the same retention time for both the undegraded aromatics and the TiO_2 photodegraded aromatic had % areas 3.102 and 1.056, respectively which confirms that it diminished in concentration and therefore it degraded by about 66 % in concentration.

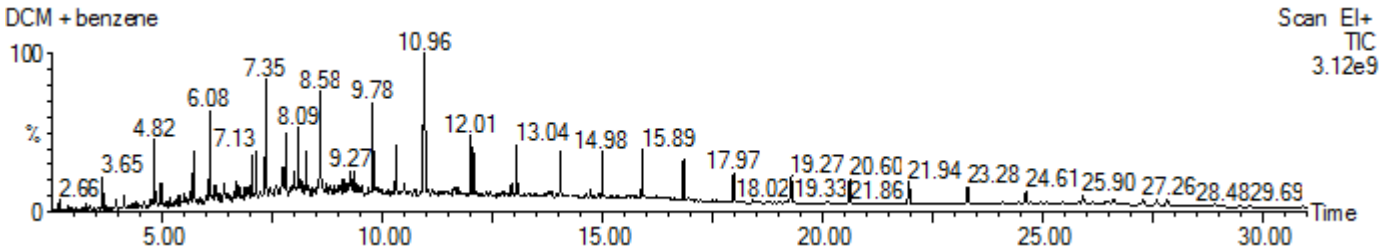

Figure 4. 13a GC/MS analyses of the mixture of DCM and the aromatic fraction of the crude oil that has not undergone degradation.

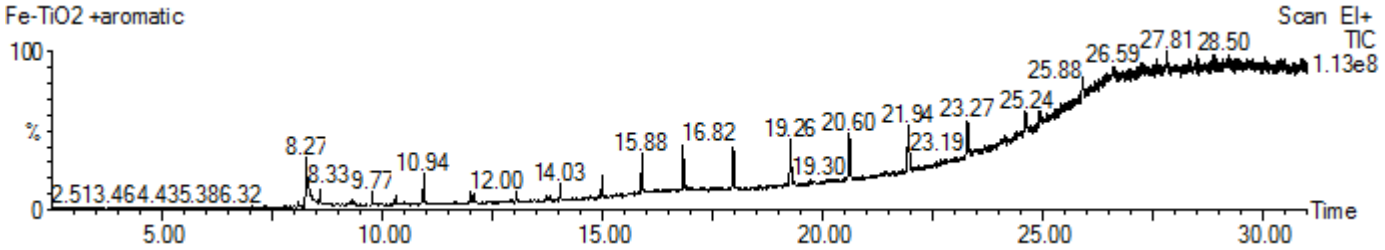

Figure 4.13b GC/MS chromatogram of the mixture of DCM and the aromatic fraction of the crude oil that has undergone photodegradation using Fe-TiO_2 photocatalyst after four (4) hours of sun irradiation.

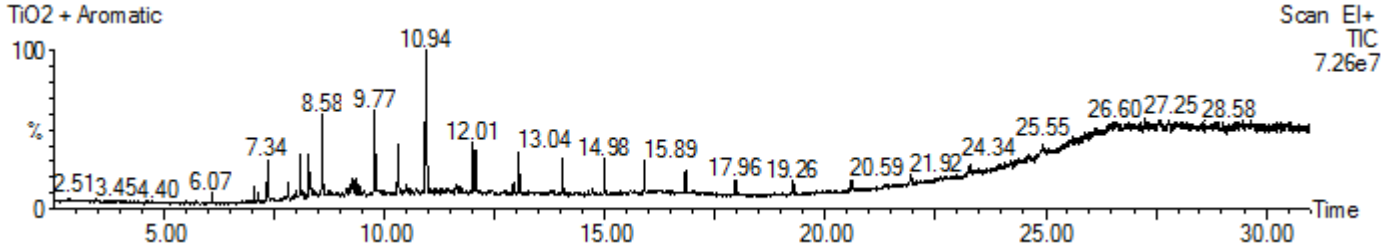

Figure 4.13c GC/MS chromatogram of the mixture of DCM and the aromatic fraction of the crude oil that has undergone degradation using TiO2 photocatalyst after four (4) hours of sun irradiation.

The GC/MS showed that some compounds which were originally in the undegraded aromatics disappeared after the Fe-TiO_2 aromatic photoproducts were analysed and compared [Table 4.8 and 4.9 in Appendix III]. The compounds that disappeared are presented in Table 4.5a below.

Table 4. 5a Compounds that disappeared with the Fe- TiO_2 photodegradation of the aromatics after four (4) hours of sunlight irradiation

#	Retention Time (RT)	Area %	Name of Compound
1	4.819	1.475	Dodecane

2	5.710	1.427	Dodecane – 4,6 – dimethyl
3	6.080	2.432	Tridecane
4	6.400	0.826	Naphthalene – 1- methyl
5	7.030	1.001	Dodecane – 2,6,10 – trimethyl
6	7.130	1.087	Decahydro – 4,4,8,9,10 penta methyl naphthalene
7	7.345	3.102	Tetradecane
8	7.745	0.880	Naphthalene 1,4 dimethyl
9	7.800	1.591	Decahydro – 4,4,8,9,10 penta methyl naphthalene
10	7.996	0.867	Naphthalene 1,3 dimethyl
11	8.091	1.861	Heptadecane 2,6,10,14 trimethyl

The GC/MS showed that some new compounds which were not originally in the undegraded aromatics were recognised after the Fe-TiO_2 aromatic photoproducts were analysed and comparisons made [Tables 4.8 and 4.9 in Appendix III]. The new compounds are presented in the Table 4.5b below.

Table 4.5b Compounds formed with Fe-TiO_2 photodegradation of the aromatics after four (4) hour sunlight irradiation.

#	Retention Time (RT)	Area %	Name of Compound
1	8.266	3.985	1 – Chloroundecane
2	10.937	1.427	Heptadecane 2,6, 10, 14 tetrametthyl
3	14.028	0.470	Heptadecane 9 – hexyl
4	14.973	0.739	Octadecane 3- ethyl-5-2 ethylbutyl
5	15.884	1.301	Heptacosane
6	16.819	1.664	Heptacosane
7	17.960	1.955	Tetratetracontane
8	19.260	2.117	Heptacosane
9	20.596	2.510	Tetratetracontane
10	21.936	2.381	Tetratetracontane
11	23.272	2.169	Tetrapentacontane-1,54-dibromo
12	23.457	0.759	Unidentified Complex Mixtures (UCM's)
13	24.592	1.812	Pentatriacontane

The GC/MS showed that some compounds which were originally in the undegraded aromatics disappeared after the TiO_2 aromatic photoproducts were analysed and comparisons were made [Tables 4.8 and 4.10 in Appendix III]. The new compounds are presented in the Table 4.5c below.

Table 4.5c Compounds that disappeared with TiO_2 photodegradation of the aromatics after four (4) hours of sunlight irradiation.

#	Retention Time (RT)	Area %	Name of Compound
1	4.819	1.475	Dodecane
3	6.080	2.432	Tridecane
4	6.400	0.826	Naphthalene – 1- methyl
5	7.030	1.001	Dodecane – 2,6,10 – trimethyl
6	7.130	1.087	Decahydro – 4,4,8,9,10 penta methyl naphthalene

The GC/MS revealed that some compounds which were not originally in the undegraded aromatics were discovered after the TiO_2 aromatic photoproducts were analysed and comparisons made [Tables 4.8 and 4.10 in Appendix III]. The new compounds are presented in the Table 4.5d below.

Table 4.5d Compounds formed with TiO_2 photodegradation of the aromatics after four (4) hour sunlight irradiation.

#	Retention Time (RT)	Area %	Name of Compound
2	7.801	0.564	1-{2-[3-(2-Acetyloxiran-2-yl)-1,1-dimethylpropyl cycloprop-2-enl} ethanone
3	8.091	1.174	Heptadecane 2,6,10,14 tetramethyl
4	8.271	2.100	1 – (2- hydroxyethyl)-1,2,5,5 tetramethyl – Cis – decalin (1R,2S,4as,8as)

5	8.581	2.158	Hydroxylamine O –decyl
6	9.266	0.700	Ethanol 2-9-Octadecenyloxy-(Z)-
7	9.341	0.680	Ethanol 2- (Octadecyloxy)
10	10.502	0.635	Z-5-Methyl-6-henecosen-1-one
14	12.928	0.557	Heptadecane 9-hexyl
15	13.043	1.211	1-Decanol, 2-hexyl
16	14.033	0.994	1-hexadecanol 2-methyl
17	14.983	0.954	Octadecane – 3- ethyl-5 -2 ethylbutyl
18	15.889	0.919	Octadecane – 3- ethyl-5 -2 ethylbutyl
19	16.829	0.779	Octadecane – 3- ethyl-5 -2 ethylbutyl
20	17.960	0.764	Octadecane – 3- ethyl-5 -2 ethylbutyl
21	19.260	0.671	Octadecane – 3- ethyl-5 -2 ethylbutyl
22	20.596	0.644	Octadecane – 3- ethyl-5 -2 ethylbutyl
23	21.946	0.647	Tetrapentacontane1,54 dibromo

4.4.3.2 GC/MS ANALYSIS OF THE ASPHALTINIC PHOTOPRODUCTS

Figures 4.13 (d-f) is the GC/MS spectra obtained from the photodegradation of the asphaltinic fraction of the crude oil using TiO_2 and Fe-TiO_2 photocatalysts. Figures 4.13(e - f) shows the UCM's has been resolved compared to Figure 4.13d that has a hump of UCM's at the end. There is also the formation of new peaks at the lower retention times in Figures

4.13(e – f) than in Figure 4.13d. All these are evident of photodegradation of the asphaltenes [83, 85]. Comparing Figures 4.13(e and f) it can be observed that Fe-TiO_2+asphaltenes degraded more, showing the formation of more new peaks than the TiO_2+asphaltenes. This also confirms that the Fe-TiO_2 is more efficient than TiO_2 in degrading the asphaltinic fraction of the crude oil under sunlight irradiation. This is evident also in the FTIR in Figure 4.12g in appendix II and UV-Vis spectra in Figure 4.12g in Appendix I.

The Fe- TiO_2 and TiO_2 was able to resolve a lot of the UCM's in the undegraded asphaltenes after four (4) hours of sunlight irradiation as is evidenced in the Tables 4.12 and 4.13 in appendix III. This is evidence of the photodegradation of the asphaltenes by the Fe-TiO_2 and the TiO_2. Comparing Tables 4.11 and 4.12 in the Appendix III it is evident that the Fe-TiO_2 was better at resolving the UCM's in the undegraded asphaltenes than the TiO_2. Fe-TiO_2 photocatalyst eluted some compounds at a lower retention time of 6.070 as opposed to that of the TiO_2 at 7.745. Again, it can be inferred from the above deductions that the Fe-TiO_2 is better at photodegrading the asphaltenes than the TiO_2.

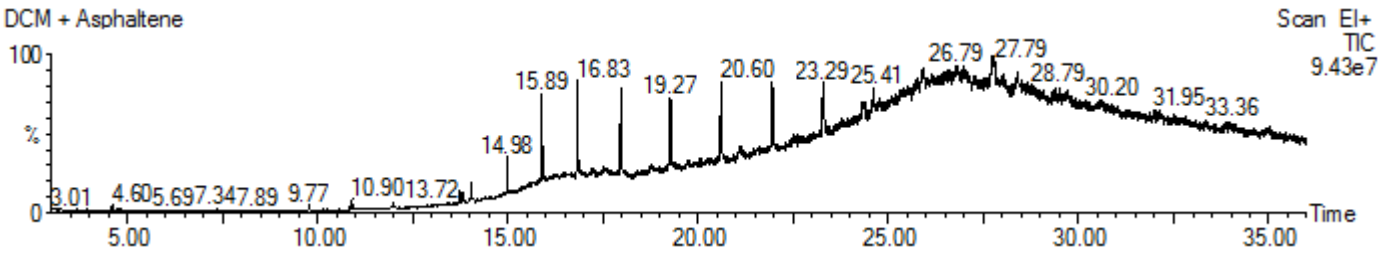

Figure 4.13d GC/MS chromatogram of the mixture of DCM and the asphaltinic fraction of the crude oil that has not undergone degradation.

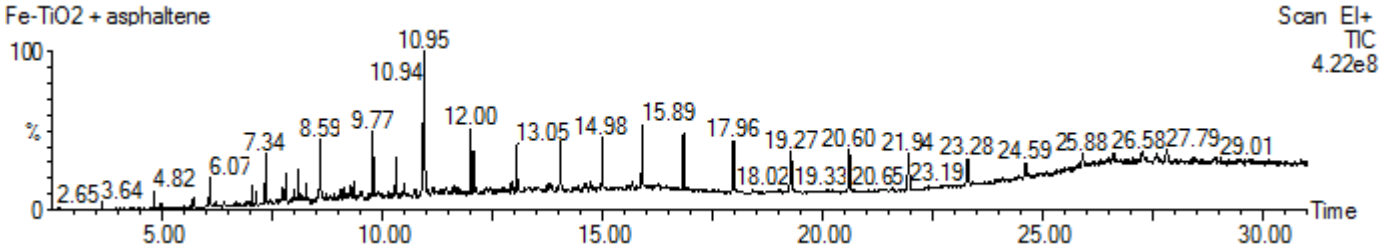

Figure 4.13e GC/MS chromatogram of the mixture of DCM and the asphaltinic fraction of the crude that has undergone degradation using Fe-TiO_2 photocatalyst after four (4) hours of sun irradiation.

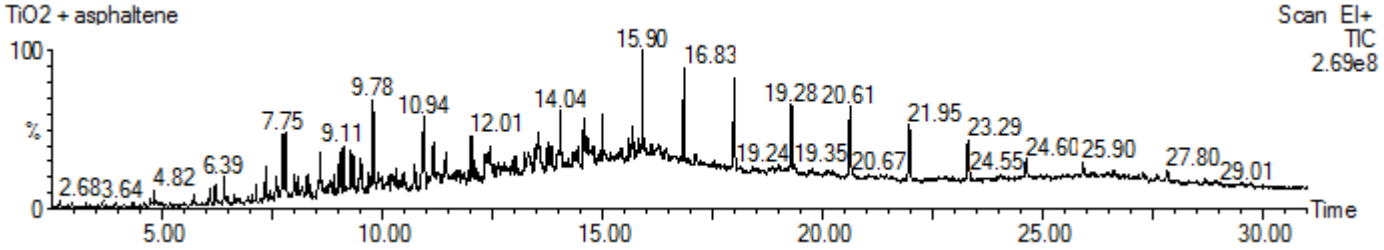

Figure 4.13f GC/MS chromatogram of the mixture of DCM and the asphaltinic fraction of the crude that has undergone degradation using TiO_2 photocatalyst after four (4) hours of sun irradiation.

4.4.3.3 GC/MS ANALYSIS OF THE PARAFFINIC PHOTOPRODUCTS

Unidentified complex mixtures (UCM'S) after the four (4) hour sunlight irradiation of the paraffins with the Fe-TiO_2 and TiO_2 photocatalysts were observed in Tables 4.15 and 4.16 in Appendix III, respectively indicating degradation of the paraffinic fraction.

New compounds were also formed when Fe-TiO_2 photocatalyst was used to photodegrade the paraffins. These new compounds were different from the ones identified in the undegraded paraffins (Table 4.14 in Appendix III) and are presented in Table 4.6a.

The compounds that disappeared after photocatalytic degradation of the paraffins fraction by TiO_2 and Fe-TiO_2 photocatalysts are presented in Tables 4.6a and 4.6c, respectively.

Again Figures 4.13(g – i) are the GC/MS that shows the gas chromatograms obtained for the photodegradation of the paraffinic fraction of the crude oil using TiO_2 and Fe-TiO_2 photocatalysts. Figure 4.13(h) shows that as compared to the Figure 4.13g most of the peaks disappeared , hence a hump of unresolved complex mixtures (UCM's) which is evident of severe photodegration of the paraffins by the Fe-TiO_2 can be observed. Again comparing Figure 4.13i to that of the Figure 4.13g some significant changes in the peaks with new ones forming and some missing and some UCM also forming, also indicates some level of photodegration [83, 85]. Comparing Figures 4.11(h and i), it can be observed that Fe-TiO_2 degraded more of the paraffins, showing more diminished, missing and UCM's peaks which indicates severe degradation than the TiO_2. This observation is again evident in the FTIR in Figure 4.12b and the UV-Vis spectra in Figure 4.11b.

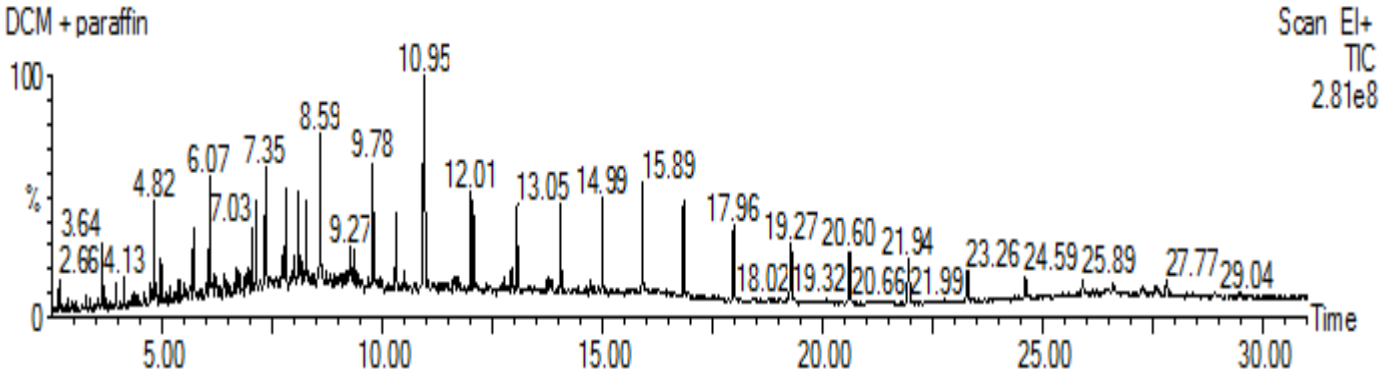

Figure 4.13g GC/MS chromatogram of the mixture of DCM and the paraffinic fraction of the crude oil that has undergone degradation using TiO_2 photocatalyst after four (4) hours of sun irradiation.

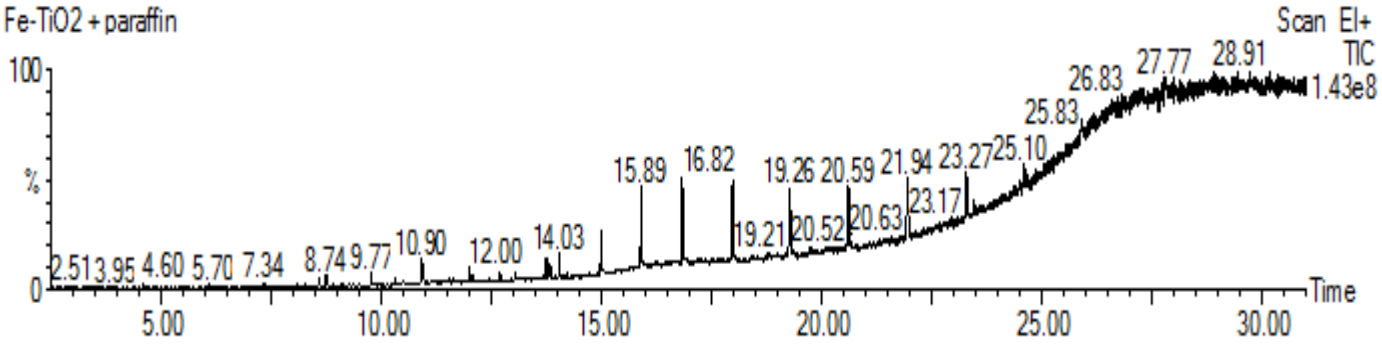

Figure 4.13h GC/MS chromatogram of the mixture of DCM and the paraffinic fraction of the crude oil that has undergone degradation using Fe - TiO_2 photocatalyst after four (4) hours of sun irradiation

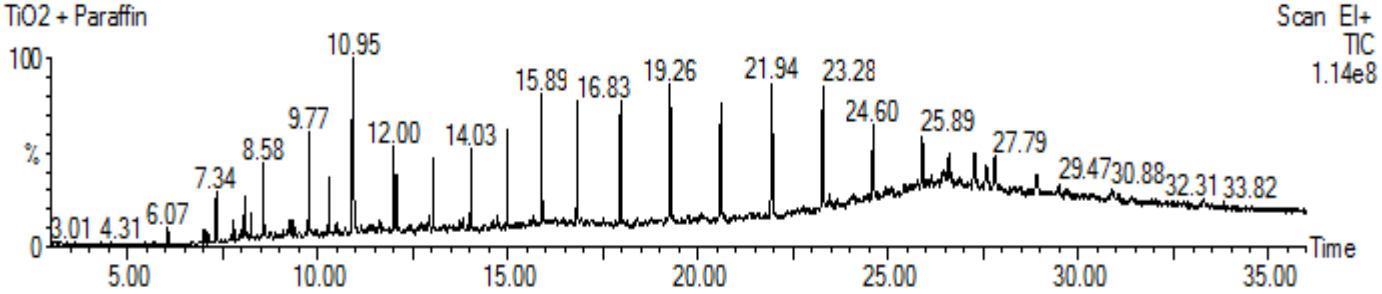

Figure 4.13i GC/MS chromatogram of the mixture of DCM and the paraffinic fraction of the crude oil that has undergone degradation using TiO_2 photocatalyst after four (4) hours of sun irradiation

In the qualitative report of the GC/MS it showed that some compounds which were originally in the undegraded paraffins disappeared after the Fe-TiO_2 paraffinic photoproducts were analysed and comparisons made (Tables 14 and 15 in Appendix III). The new compounds are presented in the Table 4.6a below.

Table 4. 6a Compounds that disappeared with Fe- TiO_2 photodegradation of the paraffins after four (4) hours of sunlight irradiation.

#	Retention Time (RT)	Area %	Name of Compound
1	3.644	0.708	Undecane

2	4.819	1.533	Dodecane
3	4.969	0.734	1-Octanol-2-butyl
4	5.710	1.147	Dodecane 4,6 dimethyl
5	6.075	1.857	Tridecane
6	6.190	0.637	Benzocycloheptatriene
7	7.030	0.805	Dodecane 2,6,10 trimethyl
8	7.125	1.250	Dodecane 2,6,10 trimethyl
9	7.345	2.384	Decahydro-4,4,8,9,10 pentamethylnaphthalene
10	7.745	0.688	Tetradecane
11	7.800	1.606	Naphthalene 1,8-dimethyl
12	8.091	1.422	Decahydro-4,4,8,9,10 pentamethylnaphthalene
13	8.271	1.339	Dodecane 2,6,10 trimethyl
14	8.856	2.695	Decahydro-4,4,8,9,10 pentamethylnaphthalene

The GC/MS showed that some compounds which were originally in the undegraded paraffins disappeared after the Fe-TiO_2 paraffinic photoproducts were analysed and comparisons made (Tables 14 and 15 in Appendix III). The new compounds are presented in the table 4.6b below.

Table 4. 6b Compounds formed with Fe-TiO_2 photodegradation of the paraffins after four (4) hour sunlight irradiation.

#	Retention Time (RT)	Area %	Name of compound
1	9.766	0.391	Nonadecane
2	10.902	0.683	Tert-Hexadecanethiol
3	10.937	0.602	Butane 2,2 dimethyl

4	13.738	0.439	Octadecanol 2-bromo
5	13.828	0.381	2-Nonadecanone 2,4 dimitrophenylhydrazine
6	14.028	0.496	Nonadecane
7	14.978	0.981	Nonadecane
8	15.899	1.834	Heneicosane
9	16.824	2.369	Hexacosane
10	17.965	2.615	Heptacosane
11	18.770	0.437	UCM's
12	19.260	2.756	Eicosane 2-methyl
14	20.591	2.643	Octadecane 3-ethyl-5-(2-ethylbutyl-)

The GC/MS qualitative analyses showed that some compounds which were originally in the undegraded paraffins disappeared after the TiO_2 paraffins photoproducts were analysed and comparisons made (Tables 14 and 16 in Appendix III). The new compounds are presented in the table 4.6c below.

Table 4. 6c Compounds that disappeared with the TiO_2 photodegradation of the paraffins after four (4) hours of sunlight irradiation.

#	Retention Time (RT)	Area %	Name of Compound
1	3.644	0.708	Undecane
2	4.819	1.533	Dodecane
3	4.969	0.734	1-Octanol-2-butyl
4	5.710	1.147	Dodecane 4,6 dimethyl
5	6.075	1.857	Tridecane
6	6.190	0.637	Benzocycloheptatriene
9	7.345	2.384	Decahydro-4,4,8,9,10 pentamethylnaphthalene
10	7.745	0.688	Tetradecane

11	7.800	1.606	Naphthalene 1,8-dimethyl
12	8.091	1.422	Decahydro-4,4,8,9,10 pentamethylnaphthalene

The results showed that indeed TiO_2 and Fe-TiO_2 have the potential to photodegrade aromatics, paraffins and asphaltenes fractions in crude oil. The photodegradation resulted in the diminishing of the concentration of existing compounds, formation of new compounds and the disappearance of existing compounds. The Fe-TiO_2 out-performed the TiO_2 under sunlight and visible light irradiation due to the shift in the band gap of the TiO_2 from 3.12 eV to 2.9 eV for the Fe-TiO_2 and the enhanced absorption in the visible light region as was observed from the DRS results. This shift made the Fe-TiO_2 active in the visible light region. In addition, the presence of Fe in the TiO_2 structure is expected to reduce the electron-hole recombination during the photocatalysis by acting as electron trapping sites. This is expected to enhance the photocatalytic efficiency. The photodegradation of the crude oil fractions can be attributed to the generation of reactive oxygen species which in turn attacked the various compounds present in each fraction degrading them into new products. The enhanced photodegradation of the aromatic components can be attributed to their relatively higher aqueous solubility which enhanced the proximity between the aromatic compounds and the reactive oxygen species generated through the photocatalysis. The results from this study showed the potential role that Fe-TiO_2 can play in visible light photodegradation of crude oil. This suggest that, photoremediation can be used as a stand-alone oil spill remediation strategy or as an add-on oil spill remediation step to enhance the degradation of water dissolvable components in crude oil.

CHAPTER FIVE

5.0 CONCLUSIONS AND RECOMMENDATION

TiO_2 and Fe-TiO_2 were successfully synthesized by mild hydrothermal method and subsequently characterized using XRD, UV-Vis, DRS, EDX, SEM, FTIR, TGA and DSC. The results from these analyses confirmed the formation of pure anatase phase of TiO_2 and Fe-doped TiO_2. The optical bandgaps were estimated to be 3.12 eV and 2.9 eV for TiO_2 and Fe-TiO_2, respectively. This implies that while TiO_2 is active in the UV region of the electromagnetic spectrum, Fe-TiO_2 is active in the visible light region of the electromagnetic spectrum. The crystallite sizes computed using the Debye Scherers equation was respectively 4.1 nm and 3.5 nm for the synthesized TiO_2 and Fe-TiO_2. SEM images depicted the formation of chunky uneven particles for both the TiO_2 and Fe-TiO_2 and this was attributed to the grinding of the particles after drying. The TGA/DSC results showed that the synthesized photocatalysts were stable even above temperature of 400 °C. Crude oil was separated into three bulk fractions; the aromatics, asphaltenes and the paraffins and each fraction subjected to photocatalysis under UV, sunlight and visible light irradiation for 4 hours. It was revealed that the as-prepared TiO_2 and the Fe-TiO_2 were able to degrade the fractions of the crude oil after four (4) hours of irradiation from the various light sources employed in this work. The Fe-TiO_2 showed a higher efficiency in the photocatalytic degradation of the fractionated crude oil samples than the TiO_2 in the presence of sunlight and visible light. This was due to the redshift in the Fe-TiO_2 by Fe^{3+} dopant. However, under UV light source, TiO_2 was more efficient than the Fe-TiO_2. It was again realized that TiO_2 and Fe-TiO_2 degraded more of the aromatics and at faster rate than the paraffins and asphaltenes as opposed to biodegradation of the same fractions which is reported in literature to be faster than aromatics. The results show the potential of photoremediation in oil spill remediation.

For future work, synthetic sea should be used instead of distilled water to examine the effect of salt ions on the photodegradation process. In addition, the photocatalyst loading as well as the irradiation time should be varied to examine their effect on photodegradation. Since different intermediate photoproducts were formed, toxicological studies of the entire photodegradation process should be carried out. A combined photoremediation and bioremediation system should be developed by combined a photocatalyst and a chemical dispersant.

REFERENCES.

1. Nyankson, E., M.J. DeCuir, and R.B. Gupta, *Soybean lecithin as a dispersant for crude oil spills.* ACS Sustainable Chemistry & Engineering, 2015. **3**(5): p. 920-931.
2. Mills, A. and S. Le Hunte, *An overview of semiconductor photocatalysis.* Journal of photochemistry and photobiology A: Chemistry, 1997. **108**(1): p. 1-35.
3. Chong, M.N., et al., *Recent developments in photocatalytic water treatment technology: a review.* Water research, 2010. **44**(10): p. 2997-3027.
4. Santos, R.d.S., et al., *Iron insertion and hematite segregation on Fe-doped TiO2 nanoparticles obtained from sol–gel and hydrothermal methods.* ACS applied materials & interfaces, 2012. **4**(10): p. 5555-5561.
5. Fujishima, A., X. Zhang, and D.A. Tryk, *Heterogeneous photocatalysis: from water photolysis to applications in environmental cleanup.* International journal of hydrogen energy, 2007. **32**(14): p. 2664-2672.
6. Herrmann, J.-M., *Heterogeneous photocatalysis: fundamentals and applications to the removal of various types of aqueous pollutants.* Catalysis today, 1999. **53**(1): p. 115-129.
7. Fujishima, A., T.N. Rao, and D.A. Tryk, *Titanium dioxide photocatalysis.* Journal of photochemistry and photobiology C: Photochemistry reviews, 2000. **1**(1): p. 1-21.
8. Gaya, U.I. and A.H. Abdullah, *Heterogeneous photocatalytic degradation of organic contaminants over titanium dioxide: a review of fundamentals, progress and problems.* Journal of Photochemistry and Photobiology C: Photochemistry Reviews, 2008. **9**(1): p. 1-12.
9. Fujishima, A. and X. Zhang, *Titanium dioxide photocatalysis: present situation and future approaches.* Comptes Rendus Chimie, 2006. **9**(5-6): p. 750-760.
10. Huang, F., A. Yan, and H. Zhao, *Influences of doping on photocatalytic properties of TiO2 photocatalyst*, in *Semiconductor Photocatalysis-Materials, Mechanisms and Applications*2016, InTech.
11. Ajaj, B.M.A.-S.E.A., *Urea Modified TiO_2 Nanoparticles Prepared by Sol-Gel Method to enhance the Photocatalytic Activity under Sunlight.* Eng. & Tech.Journal, 2015. **Vol. 33**(Part(B)).
12. Department, E., *What is crude oil? A detailed Explanation on this essential fossil fuel.*, in *Oilprice.com*2009, Oilprice: US.
13. Board, M., O.S. Board, and N.R. Council, *Oil in the sea III: inputs, fates, and effects*2003: national academies Press.
14. Gary, J.H., G.E. Handwerk, and M.J. Kaiser, *Petroleum refining: technology and economics*2007: CRC press.
15. Wikimedia.org, *Colour of Crude oils.*
16. Rybak, B., *Analysis of Petroleum and Petroleum Products.* Gostoptekhizdat, Moscow, 1962.
17. Atlas, R., *Effects of temperature and crude oil composition on petroleum biodegradation.* Applied microbiology, 1975. **30**(3): p. 396-403.
18. Speight, J.G., *The chemistry and technology of petroleum*2014: CRC press.
19. Freund, M., *Paraffin products: properties, technologies, applications*. Vol. 14. 1982: Elsevier Science Limited.
20. Nyankson, E., et al., *Surfactant-loaded halloysite clay nanotube dispersants for crude oil spill remediation.* Industrial & Engineering Chemistry Research, 2015. **54**(38): p. 9328-9341.
21. Etkin, D.S. *Analysis of oil spill trends in the United States and worldwide*. in *International Oil Spill Conference*. 2001. American Petroleum Institute.
22. Aske, N., H. Kallevik, and J. Sjöblom, *Determination of saturate, aromatic, resin, and asphaltenic (SARA) components in crude oils by means of infrared and near-infrared spectroscopy.* Energy & Fuels, 2001. **15**(5): p. 1304-1312.

23. Karl, T.L., *Understanding the resource curse.* Covering Oil: A Guide to Energy and Development, 2005: p. 21-27.
24. Sunmoni, M., *Oil Spills: Causes, Effects and Control.* 2012.
25. Garrett, R.M., et al., *Photooxidation of crude oils.* Environmental Science & Technology, 1998. **32**(23): p. 3719-3723.
26. Muizis, A., *Evaluation of the Methods for the Oil Spill Response in the Offshore Arctic Region*, in *Environmental Engineering*2013, Helsinki Metropolia University of Applied Sciences: theseus.fi.
27. Mullin, J.V. and M.A. Champ, *Introduction/Overview to In Situ Burning of Oil Spills.* Spill Science & Technology Bulletin, 2003. **8**(4): p. 323-330.
28. Doerffer, J.W., *Oil spill response in the marine environment*2013: Elsevier.
29. Milwidsky, B., et al., *CRUDE OIL: LIQUID CHROMATOGRAPHY.* Journal of the American Oil Chemists' Society, 2000. **72**(1): p. 9.
30. Mortada, I., *Chromatography-part 4*, 2009.
31. Made-in-china, *heb-instrument*, N.R.E.w.d. RE, Editor 2018.
32. Zhang, L., et al., *Photocatalytic degradation of polycyclic aromatic hydrocarbons on soil surfaces using TiO2 under UV light.* Journal of Hazardous Materials, 2008. **158**(2-3): p. 478-484.
33. Hsu, Y.-Y., et al., *Photocatalytic degradation of spill oils on TiO2 nanotube thin films.* Marine pollution bulletin, 2008. **57**(6-12): p. 873-876.
34. Macwan, D., P.N. Dave, and S. Chaturvedi, *A review on nano-TiO2 sol–gel type syntheses and its applications.* Journal of Materials Science, 2011. **46**(11): p. 3669-3686.
35. Insertion, I., *Hematite Segregation on Fe-Doped TiO2 Nanoparticles Obtained from Sol-Gel and Hydrothermal Methods Santos.* Reginaldo da S: p. 5555-5561.
36. Wu, J.-M. and T.-W. Zhang, *Photodegradation of rhodamine B in water assisted by titania films prepared through a novel procedure.* Journal of Photochemistry and Photobiology A: Chemistry, 2004. **162**(1): p. 171-177.
37. Xing, J., et al., *Inorganic photocatalysts for overall water splitting.* Chemistry–An Asian Journal, 2012. **7**(4): p. 642-657.
38. Lu, M., *Photocatalysis and water purification: from fundamentals to recent applications*2013: John Wiley & Sons.
39. Vela, N., et al., *Removal of polycyclic aromatic hydrocarbons (PAHs) from groundwater by heterogeneous photocatalysis under natural sunlight.* Journal of Photochemistry and Photobiology A: Chemistry, 2012. **232**: p. 32-40.
40. Woo, O., et al., *Photocatalytic oxidation of polycyclic aromatic hydrocarbons: intermediates identification and toxicity testing.* Journal of Hazardous Materials, 2009. **168**(2-3): p. 1192-1199.
41. Dong, D., et al., *Photocatalytic degradation of phenanthrene and pyrene on soil surfaces in the presence of nanometer rutile TiO2 under UV-irradiation.* Chemical Engineering Journal, 2010. **158**(3): p. 378-383.
42. Lee, S.-Y. and S.-J. Park, *TiO2 photocatalyst for water treatment applications.* Journal of Industrial and Engineering Chemistry, 2013. **19**(6): p. 1761-1769.
43. Ba-Abbad, M.M., et al., *Synthesis and catalytic activity of TiO2 nanoparticles for photochemical oxidation of concentrated chlorophenols under direct solar radiation.* Int. J. Electrochem. Sci, 2012. **7**: p. 4871-4888.
44. Hara, K., et al., *Molecular design of coumarin dyes for efficient dye-sensitized solar cells.* The Journal of Physical Chemistry B, 2003. **107**(2): p. 597-606.
45. Lim, C.S., et al., *Reaction morphology and the effect of pH on the preparation of TiO 2 nanoparticles by a sol-gel method.* Journal of Ceramic Processing Research, 2010. **11**(6): p. 736-741.

46. Edelstein, A.S. and R. Cammaratra, *Nanomaterials: synthesis, properties and applications*1998: CRC press.
47. Chi, L.H., *Hydothermal synthesis and enhanced photocatalytic activity of TiO_2 -Fe and CNT_s Nanacomposite for methylene blue degradation under visible light irradiation.* 2014.
48. Xu, J., et al., *Nanocrystalline N-Doped Powders: Mild Hydrothermal Synthesis and Photocatalytic Degradation of Phenol under Visible Light Irradiation.* International Journal of Photoenergy, 2013. **2013**.
49. Malekshahi Byranvand, M., et al., *A review on synthesis of nano-TiO2 via different methods.* Journal of nanostructures, 2013. **3**(1): p. 1-9.
50. Caratto, V., et al., *Different sol–gel preparations of iron-doped TiO2 nanoparticles: characterization, photocatalytic activity and cytotoxicity.* Journal of Sol-Gel Science and Technology, 2016. **80**(1): p. 152-159.
51. Asahi, R., et al., *Visible-light photocatalysis in nitrogen-doped titanium oxides.* science, 2001. **293**(5528): p. 269-271.
52. Jafari, T., et al., *Photocatalytic water splitting—the untamed dream: a review of recent advances.* Molecules, 2016. **21**(7): p. 900.
53. Khan, H. and I.K. Swati, *Fe3+-doped anatase TiO2 with d–d transition, oxygen vacancies and Ti3+ centers: synthesis, characterization, UV–vis photocatalytic and mechanistic studies.* Industrial & Engineering Chemistry Research, 2016. **55**(23): p. 6619-6633.
54. Sood, S., et al., *Highly effective Fe-doped TiO2 nanoparticles photocatalysts for visible-light driven photocatalytic degradation of toxic organic compounds.* Journal of colloid and interface science, 2015. **450**: p. 213-223.
55. Mahshid, S., M. Askari, and M.S. Ghamsari, *Synthesis of TiO2 nanoparticles by hydrolysis and peptization of titanium isopropoxide solution.* Journal of Materials Processing Technology, 2007. **189**(1-3): p. 296-300.
56. Kavitha, M., C. Gopinathan, and P. Pandi, *Synthesis and characterization of TiO2 nanopowders in hydrothermal and Sol-Gel method.* International Journal of Advancements in Research & Technology, 2013. **2**(4): p. 102-108.
57. M. Cerma, C.G., E. Puzenat, M. Vesely & P. Dzik, *Hydrothermal synthesis of TiO_2 : Influences of process conditions on photocatalytic activity.* International Journal of Chem. Environment. Eng., 2011. **Vol. 2**(4).
58. Bao, N., et al., *Low-temperature hydrothermal synthesis of N-doped TiO2 from small-molecule amine systems and their photocatalytic activity.* Environmental technology, 2013. **34**(21): p. 2939-2949.
59. Wu, D., et al., *Low temperature hydrothermal synthesis of N-doped TiO2 photocatalyst with high visible-light activity.* Journal of Alloys and Compounds, 2010. **502**(2): p. 289-294.
60. Swapp, S., *Scanning electron microscopy (SEM).* Geochemical Instrumentation and Analysis, 2012.
61. Perkins, W., *Fourier transform-infrared spectroscopy: Part I. Instrumentation.* Journal of Chemical Education, 1986. **63**(1): p. A5.
62. Griffiths, P.R. and J.A. De Haseth, *Fourier transform infrared spectrometry*. Vol. 171. 2007: John Wiley & Sons.
63. Saptari, V., *Fourier transform spectroscopy instrumentation engineering*2003: SPIE Optical Engineering Press.
64. Smith, B.C., *Fundamentals of Fourier transform infrared spectroscopy*2011: CRC press.
65. Kubelka, P. and F. Munk, *An article on optics of paint layers.* Z. Tech. Phys, 1931. **12**(593-601).
66. Morales, A.E., E.S. Mora, and U. Pal, *Use of diffuse reflectance spectroscopy for optical characterization of un-supported nanostructures.* Revista mexicana de física, 2007. **53**(5): p. 18-22.
67. Douglas, F., *Gc/ms analysis.* Scientific Testimony-An online journal, 2004.

68. Jing, L., et al., *The surface properties and photocatalytic activities of ZnO ultrafine particles.* Applied Surface Science, 2001. **180**(3-4): p. 308-314.
69. Xu, Z., et al., *The preparation and characterization of TiO2 ultrafine particles.* Materials Science and Engineering: B, 1999. **63**(3): p. 211-214.
70. Yoon, C. and D.L. Cocke, *Potential of amorphous materials as catalysts.* Journal of non-crystalline solids, 1986. **79**(3): p. 217-245.
71. Mardare, D., et al., *On the structural properties and optical transmittance of TiO2 rf sputtered thin films.* Applied Surface Science, 2000. **156**(1-4): p. 200-206.
72. Cheng, H.-H., et al., *Sol-Gel Hydrothermal Synthesis and Visible Light Photocatalytic Degradation Performance of Fe/N Codoped TiO2 Catalysts.* Materials, 2018. **11**(6): p. 939.
73. Kim, T.-H., et al., *Synthesis of solar light responsive Fe, N co-doped TiO2 photocatalyst by sonochemical method.* Catalysis today, 2013. **212**: p. 75-80.
74. Deng, L., et al., *Synthesis, characterization of Fe-doped TiO 2 nanotubes with high photocatalytic activity.* Catalysis Letters, 2009. **129**(3-4): p. 513-518.
75. Li, Z., et al., *Effect of Fe-doped TiO2 nanoparticle derived from modified hydrothermal process on the photocatalytic degradation performance on methylene blue.* Journal of Hazardous Materials, 2008. **155**(3): p. 590-594.
76. Luu, C.L., Q.T. Nguyen, and S.T. Ho, *Synthesis and characterization of Fe-doped TiO2 photocatalyst by the sol–gel method.* Advances in Natural Sciences: Nanoscience and Nanotechnology, 2010. **1**(1): p. 015008.
77. Yu, J., X. Zhao, and Q. Zhao, *Effect of surface structure on photocatalytic activity of TiO2 thin films prepared by sol-gel method.* Thin solid films, 2000. **379**(1-2): p. 7-14.
78. Tang, A., et al., *ZnFe2O4-TiO2 nanoparticles within mesoporous MCM-41.* The Scientific World Journal, 2012. **2012**.
79. Hu, M., et al., *The effects of atmosphere and calcined temperature on photocatalytic activity of TiO 2 nanofibers prepared by electrospinning.* Nanoscale research letters, 2013. **8**(1): p. 548.
80. Wang, J., et al., *Preparation of Fe-doped mixed crystal TiO2 catalyst and investigation of its sonocatalytic activity during degradation of azo fuchsine under ultrasonic irradiation.* Journal of colloid and interface science, 2008. **320**(1): p. 202-209.
81. García-Serrano, J., et al., *Effect of Ag doping on the crystallization and phase transition of TiO2 nanoparticles.* Current Applied Physics, 2009. **9**(5): p. 1097-1105.
82. Zhou, J., et al. *Enhanced photocatalytic activity of Fe-doped TiO2 coated on N-doped activated carbon composites for photocatalytic degradation of dyeing wastewater*. in *AIP Conference Proceedings*. 2017. AIP Publishing.
83. Abdulkadir, I., S. Uba, and M. Almustapha, *A Rapid Method of Crude Oil Analysis Using FT-IR Spectroscopy.* Nigerian Journal of Basic and Applied Sciences, 2016. **24**(1): p. 47-55.
84. Akmaz, S., et al., *The structural characterization of saturate, aromatic, resin, and asphaltene fractions of Batiraman crude oil.* Petroleum Science and Technology, 2011. **29**(2): p. 160-171.
85. Ali, M.F., A. Bukhari, and Misbah-ul-Hasan, *Structural characterization of Arabian heavy crude oil residue.* Fuel science & technology international, 1989. **7**(8): p. 1179-1208.
86. Buenrostro-Gonzalez, E., et al., *Characterization of asphaltenes and resins from problematic Mexican crude oils.* Petroleum science and technology, 2001. **19**(3-4): p. 299-316.
87. Peralta-Martinez, M., et al., *Determination of functional groups in Mexican vacuum residua.* Petroleum Science and Technology, 2008. **26**(1): p. 91-100.

APPENDIX I

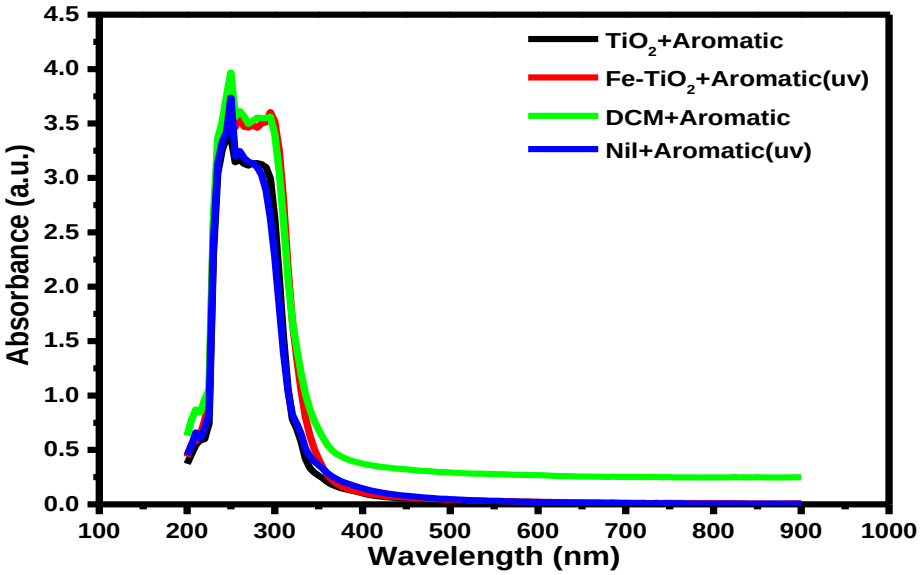

Figure 4.11e The UV-Vis spectra of the photodegraded aromatics after four (4) hours of UV light irradiation with Fe-TiO_2 photocatalyst [Fe-TiO2+Aromatic(UV)], TiO_2 photocatalyst[TiO_2+Aromatics(UV)],no photocatalyst[Nil+Aromatic(UV)].

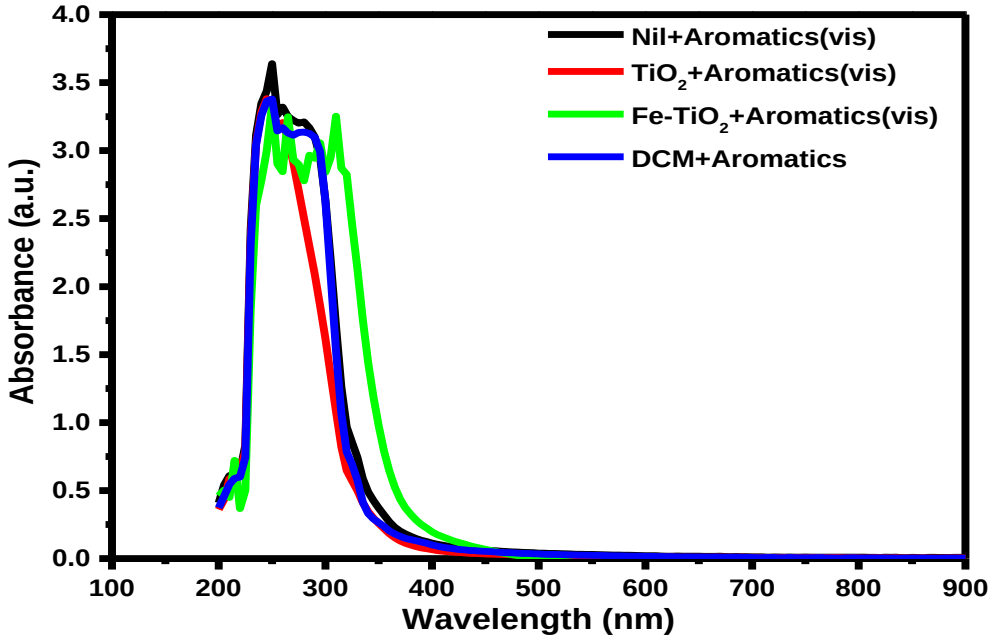

Figure 4.11f. The UV-Vis spectra of the photodegraded aromatics after four (4) hours of visible light irradiation with Fe-TiO_2 photocatalyst [Fe-TiO_2+Aromatic(Vis)], TiO_2 photocatalyst[TiO_2+Aromatics(Vis)],no photocatalyst[Nil+Aromatic(Vis)]

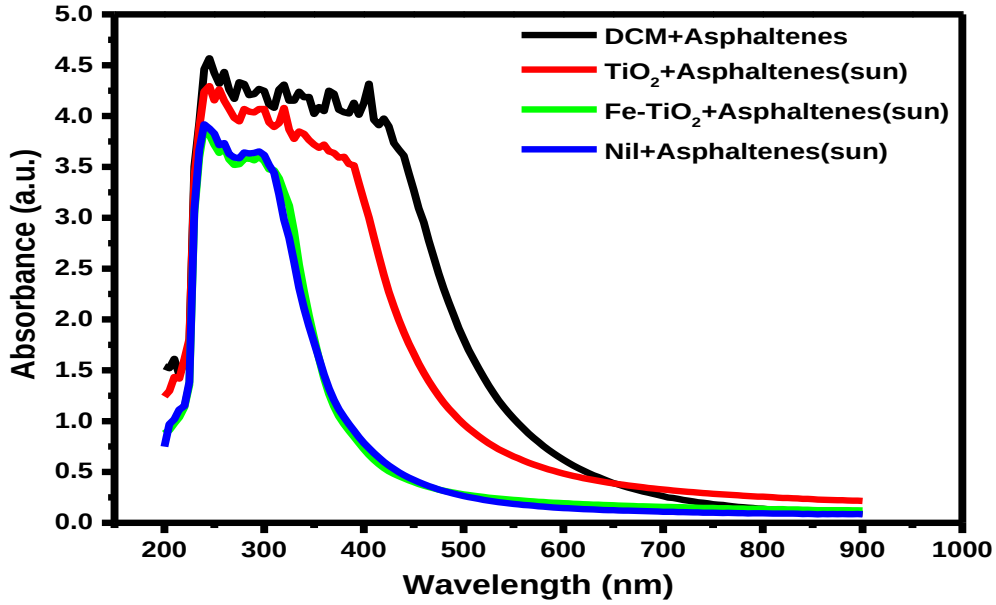

.

Figure 4.11g The UV-Vis spectra of the photodegraded asphaltenic fraction of crude oil after four (4) hours of sun irradiation with Fe-TiO_2 photocatalyst [Fe-TiO_2+ Asphaltenes (Sun)], TiO_2 photocatalyst [TiO_2+Asphaltenes (Sun)], no photocatalyst [Nil+Asphaltenes(Sun)].

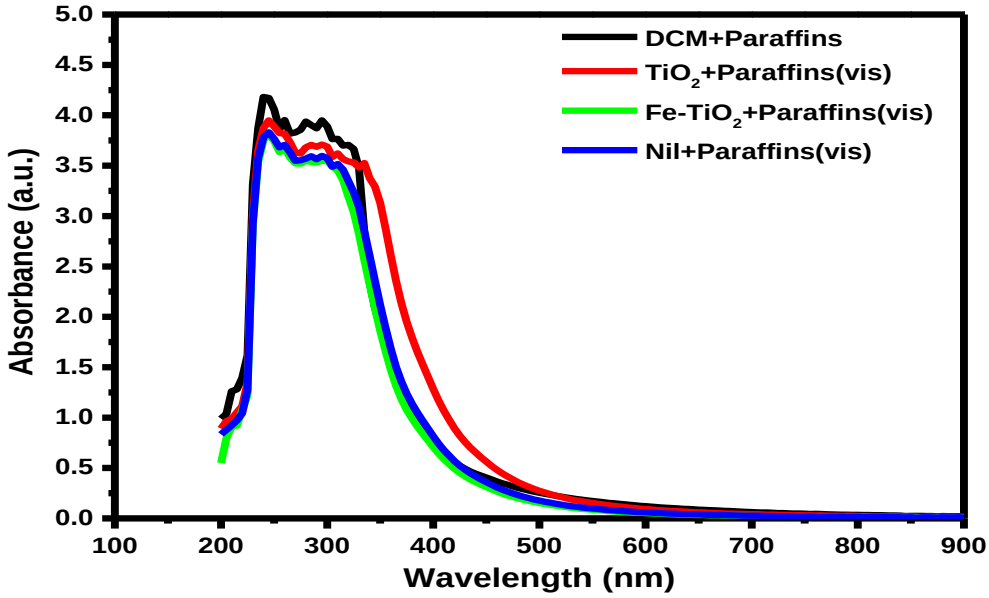

Figure 4.11h The UV-Vis spectra of the photodegraded paraffinic fraction of crude oil after four (4) hours of visible light irradiation with Fe-TiO_2 photocatalyst [Fe-TiO_2+ Paraffins (Vis)], TiO_2 photocatalyst [TiO_2+ Paraffins (Vis)], no photocatalyst [Nil+Paraffins(Vis)].

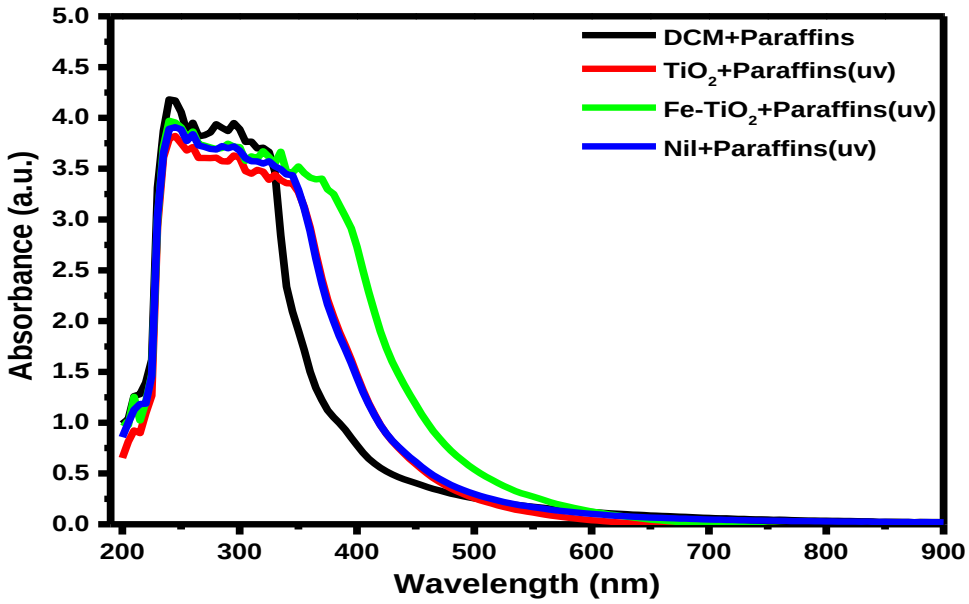

Figure 4.11i The UV-Vis spectra of the photodegraded paraffinic fraction of crude oil after four (4) hours of UV light irradiation with Fe-TiO_2 photocatalyst [Fe-TiO_2+ Paraffins (UV)], TiO_2 photocatalyst [TiO_2+Paraffins (UV)], no photocatalyst [Nil+Paraffins(UV)]

APPENDIX II

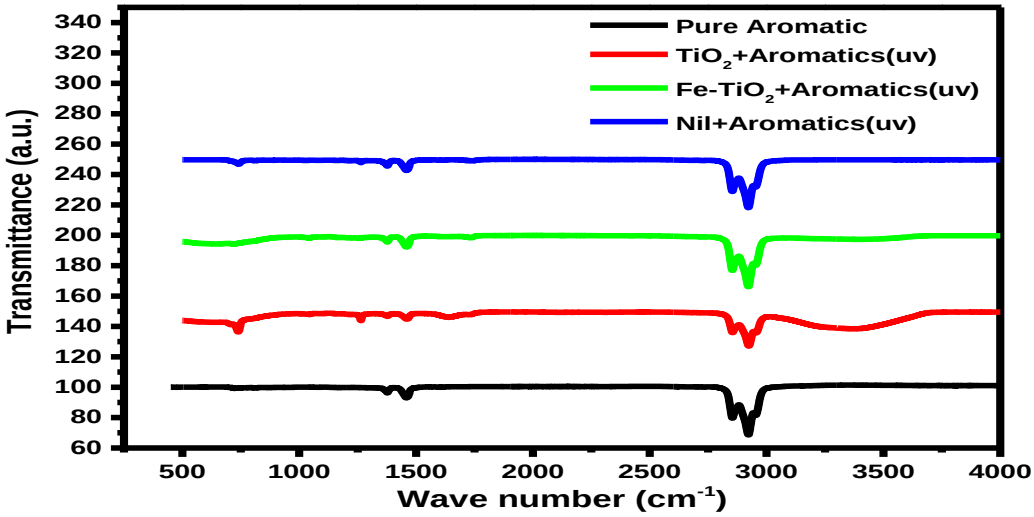

** [Pure Aromatic] is the aromatic fraction that has not undergone any degradation.

Figure 4.12e FTIR peaks of the aromatic fraction of the crude oil which was irradiated under UV light for four (4) hours using Fe-TiO_2 as photocatalyst [Fe-TiO_2+Aromatic(UV)],TiO_2 as photocatalyst [TiO_2+Aromatic(Sun)] and without photocatalyst[Nil+Aromatic(UV)].

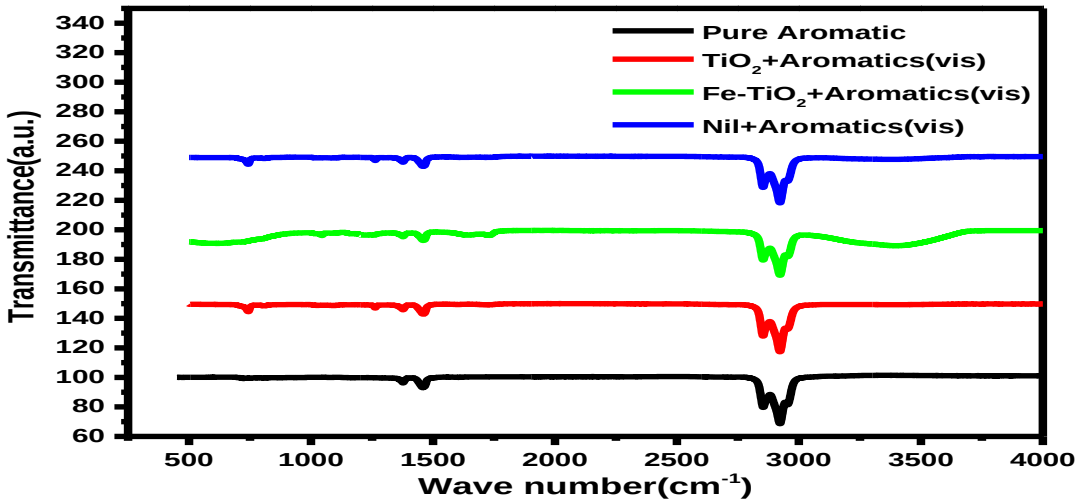

** [Pure Aromatic] is the aromatic fraction that has not undergone any degradation.

Figure 4.12f FTIR peaks of the aromatic fraction of the crude oil which was irradiated under visible light for four (4) hours using Fe-TiO_2 as photocatalyst [Fe-TiO_2+Aromatic(Vis)],TiO_2 as photocatalyst [TiO_2+Aromatic(Vis)] and without photocatalyst[Nil+Aromatic(Vis)]

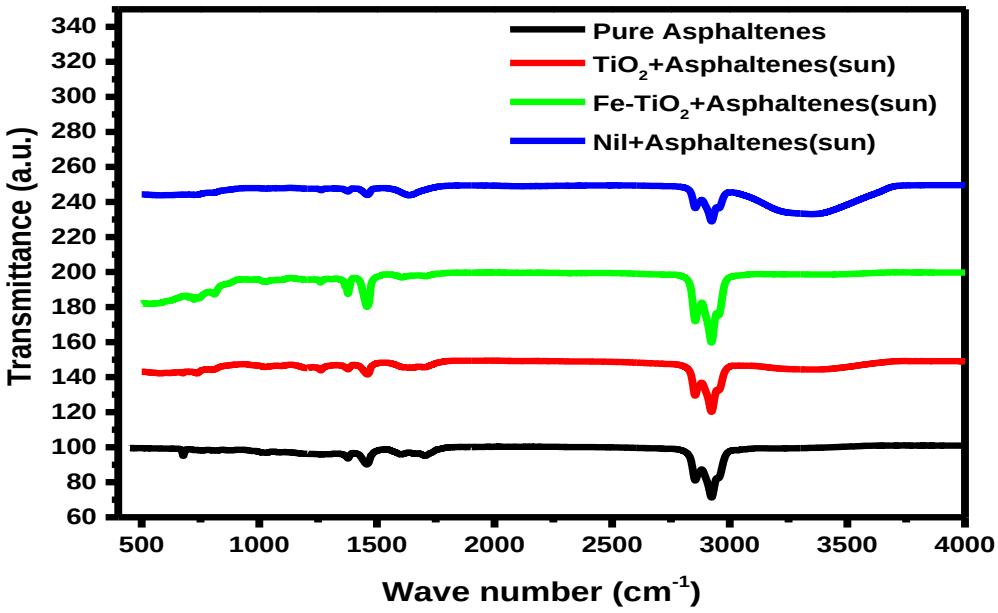

** [Pure Asphaltenes] is the asphaltenic fraction that has not undergone any degradation.

Figure 4.12g FTIR peaks of the asphaltinic fraction of the crude oil which was irradiated under sunlight for four (4) hours using Fe-TiO_2 as photocatalyst [Fe-TiO_2+Asphaltenes(Sun)],TiO_2 as photocatalyst [TiO_2+Asphaltenes(Sun)] and without photocatalyst[Nil+Asphaltenes(Sun)]

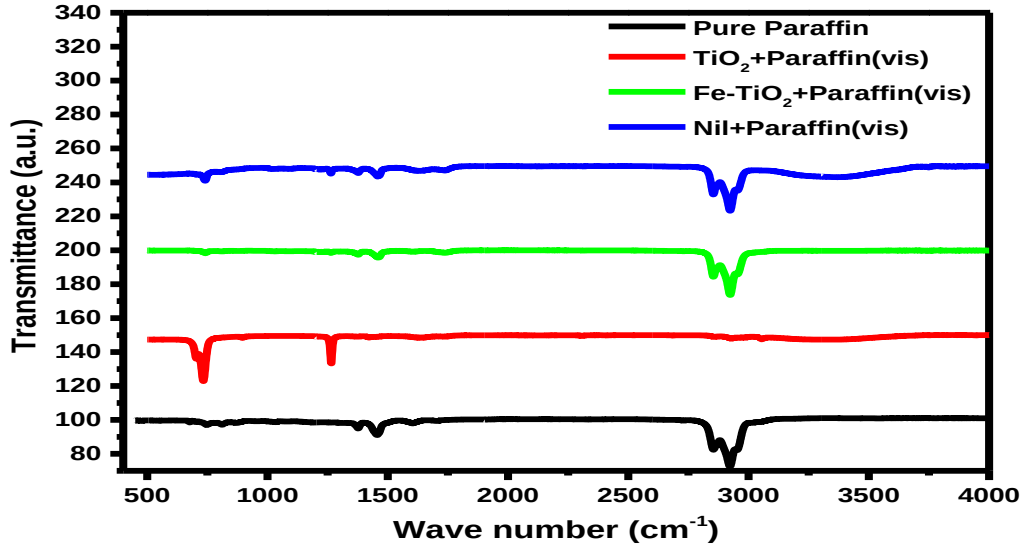

[Pure Paraffins] is the paraffins fraction that has not undergone any degradation.

Figure 4.12h FTIR peaks of the paraffinic fraction of the crude oil which was irradiated under visible light for four (4) hours using Fe-TiO_2 as photocatalyst [Fe-TiO_2+Paraffins(Vis)],TiO_2 as photocatalyst [TiO2+Paraffins(Vis)] and without photocatalyst[Nil+Paraffins(Vis)].

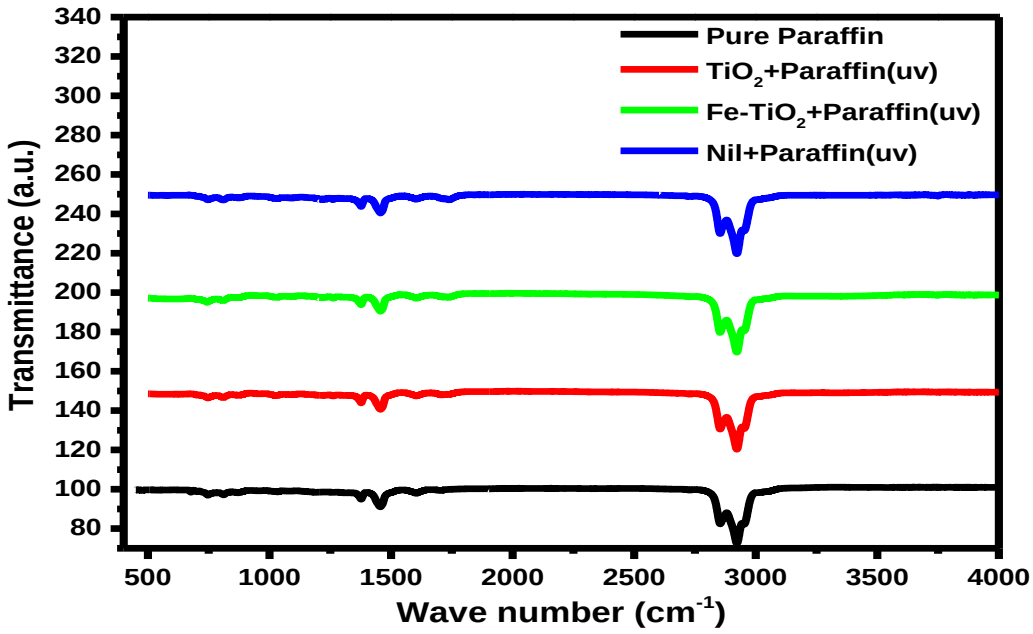

** [Pure Paraffins] is the paraffins fraction that has not undergone degradation.

Figure 4.12i FTIR peaks of the paraffinic fraction of the crude oil which was irradiated under UV light for four (4) hours using Fe-TiO_2 as photocatalyst [Fe-TiO_2+Paraffins(Sun)],TiO_2 as photocatalyst [TiO_2+Paraffins(Sun)] and without photocatalyst[Nil+Paraffins(Sun)]

APPENDIX III

Table 4.8 GC/MS qualitative analyses showing the compounds identified in the Aromatic fraction of the crude oil that has not undergone degradation.

#	Retention Time (RT)	Area %	Name of Compound
1	4.819	1.475	Dodecane
2	5.710	1.427	Dodecane – 4,6 - dimethyl
3	6.080	2.432	Tridecane
4	6.400	0.826	Naphthalene – 1- methyl
5	7.030	1.001	Dodecane – 2,6,10 - trimethyl
6	7.130	1.087	Decahydro – 4,4,8,9,10 penta methyl naphthalene
7	7.345	3.102	Tetradecane
8	7.745	0.880	Naphthalene 1,4 dimethyl
9	7.800	1.591	Decahydro – 4,4,8,9,10 penta methyl naphthalene
10	7.996	0.867	Naphthalene 1,3 dimethyl
11	8.091	1.861	Heptadecane 2,6,10,14 trimethyl
12	8.271	1.433	Decahydro – 4,4,8,9,10 penta methyl naphthalene
13	8.581	2.899	Pentadecane
14	9.776	2.427	Hexadecane
15	10.311	1.639	Pentadecane 2,6,10 trimethyl
16	10.957	6.648	Pentadecane 2,6,10,14 tetramethyl
17	12.007	1.491	Octadecane
18	12.067	1.308	Hexadecane 2,6,10,14 tetramethyl
19	13.043	1.343	Nonadecane
20	14.033	1.220	Nonadecane
21	14.983	1,257	Heneicosane

22	15.894	1.354	Heneicosane
23	16.829	1.363	Heneicosane
24	17.969	1.357	Heneicosane
25	19.270	1.234	Heneicosane
26	20.600	1.275	Hexacosane
27	21.941	1.122	Octaacosane
28	23.287	0.878	Pentacosane
29	24.607	0.735	Octacosane
30	26.598	0.730	Alfa.21a-28,30 Bisnorhopane

Table 4.9 GC/MS qualitative analyses showing the compounds identified in the DCM mixed with the Aromatic fraction of the crude oil that has undergone photodegradation using the Fe-TiO_2 photocatalyst

#	Retention Time (RT)	Area %	Name of Compound
1	8.266	3.985	1 - Chloroundecane
2	10.937	1.427	Heptadecane 2,6, 10, 14 tetrametthyl
3	14.028	0.470	Heptadecane 9 - hexyl
4	14.973	0.739	Octadecane 3- ethyl-5-2 ethylbutyl
5	15.884	1.301	Heptacosane
6	16.819	1.664	Heptacosane
7	17.960	1.955	Tetratetracontane
8	19.260	2.117	Heptacosane
9	20.596	2.510	Tetratetracontane
10	21.936	2.381	Tetratetracontane
11	23.272	2.169	Tetrapentacontane-1,54-dibromo
12	23.457	0.759	Unidentified Complex Mixtures (UCM's)

13	24.592	1.812	Pentatriacontane
14	24.912	0.653	Unidentified Complex Mixtures (UCM's)
15	25.888	1.096	Unidentified Complex Mixtures (UCM's)
16	26.593	0.673	Unidentified Complex Mixtures (UCM's)
17	27.273	0.655	Unidentified Complex Mixtures (UCM's)
18	27.498	0.439	Unidentified Complex Mixtures (UCM's)
19	27.809	1.549	Unidentified Complex Mixtures (UCM's)
20	27.914	0.496	Unidentified Complex Mixtures (UCM's)
21	27.994	0.501	Unidentified Complex Mixtures (UCM's)
22	28.499	0.470	Unidentified Complex Mixtures (UCM's)
23	28.604	0.428	Unidentified Complex Mixtures (UCM's)
24	28.929	0.478	Unidentified Complex Mixtures (UCM's)
25	29.074	0.455	Unidentified Complex Mixtures (UCM's)
26	29.224	0.413	Unidentified Complex Mixtures (UCM's)
27	29.439	0.411	Unidentified Complex Mixtures (UCM's)
28	29.654	0.513	Unidentified Complex Mixtures (UCM's)
29	29.729	0.658	Unidentified Complex Mixtures (UCM's)
30	30.029	0.416	Unidentified Complex Mixtures (UCM's)

Table 4.10 GC/MS qualitative analyses showing the compounds identified in the DCM mixed with the Aromatic fraction of the crude oil that has undergone photodegradation using the TiO_2 photocatalyst.

#	Retention Time (RT)	Area %	Name of Compound
1	7.340	1.056	Tetradecane
2	7.801	0.564	1-{2-[3-(2- Acetyloxiran-2-yl)-1,1-dimethylpropyl cycloprop-2-enl} ethanone
3	8.091	1.174	Heptadecane 2,6,10,14 tetramethyl
4	8.271	2.100	1 – (2- hydroxyethyl)-1,2,5,5 tetramethyl – Cis – decalin (1R,2S,4as,8as)
5	8.581	2.158	Hydroxylamine O -decyl
6	9.266	0.700	Ethanol 2-9-Octadecenyloxy-(Z)-
7	9.341	0.680	Ethanol 2- (Octadecyloxy)
8	9.771	2.408	Hexadecane
9	10.307	1.753	Hexadecane
10	10.502	0.635	Z-5-Methyl-6-henecosen-1-one
11	10.942	6.402	Dodecane 2,6,10 trimethyl
12	12.007	1.352	Nonadecane
13	12.067	1.284	Dodecane 2,6,10 trimethyl
14	12.928	0.557	Heptadecane 9-hexyl
15	13.043	1.211	1-Decanol, 2-hexyl
16	14.033	0.994	1-hexadecanol 2-methyl
17	14.983	0.954	Octadecane – 3- ethyl-5 -2 ethylbutyl
18	15.889	0.919	Octadecane – 3- ethyl-5 -2 ethylbutyl
19	16.829	0.779	Octadecane – 3- ethyl-5 -2 ethylbutyl
20	17.960	0.764	Octadecane – 3- ethyl-5 -2 ethylbutyl
21	19.260	0.671	Octadecane – 3- ethyl-5 -2 ethylbutyl

22	20.596	0.644	Octadecane – 3- ethyl-5 -2 ethylbutyl
23	21.946	0.647	Tetrapentacontane1,54 dibromo
24	23.292	0.710	Unidentified Complex Mixtures (UCM's)
25	24.602	0.577	Unidentified Complex Mixtures (UCM's)
26	24.938	0.589	Unidentified Complex Mixtures (UCM's)
27	27.253	0.451	Unidentified Complex Mixtures (UCM's)
28	27.549	0.444	Unidentified Complex Mixtures (UCM's)
29	27.799	0.852	Unidentified Complex Mixtures (UCM's)
30	28.899	0.596	Unidentified Complex Mixtures (UCM's)

Table 4.11 GC/MS qualitative analyses showing the compounds identified in the Asphaltinic fraction of the crude oil that has not undergone degradation.

#	Retention Time (RT)	Area %	Name of Compound
1	17.974	0.710	Octadecane, 2-methyl-
2	23.287	0.989	Octadecane, 3-ethyl-5-(2-ethylbutyl)
3	24.077	1.230	Unidentified Complex Mixtures (UCM's)
4	24.322	1.044	Unidentified Complex Mixtures (UCM's)
5	24.602	1.478	Octadecane , 3-ethyl-5-(2-ethylbuthyl)
6	24.772	1.176	Unidentified Complex Mixtures (UCM's)
7	25.177	3.130	Unidentified Complex Mixtures (UCM's)
8	25.412	2.395	Unidentified Complex Mixtures (UCM's)
9	25.502	1.648	Unidentified Complex Mixtures (UCM's)
10	25.772	2.141	Unidentified Complex Mixtures (UCM's)
11	25.913	3.285	Unidentified Complex Mixtures (UCM's)
12	26.143	3.515	Unidentified Complex Mixtures (UCM's)
13	26.788	7.463	Unidentified Complex Mixtures (UCM's)

14	26.968	3.600	Unidentified Complex Mixtures (UCM's)
15	27.248	2.486	Unidentified Complex Mixtures (UCM's)
16	27.483	1.019	Unidentified Complex Mixtures (UCM's)
17	27.783	8.176	Unidentified Complex Mixtures (UCM's)
18	28.239	1.068	Unidentified Complex Mixtures (UCM's)
19	28.394	2.703	Unidentified Complex Mixtures (UCM's)
20	28.539	2.077	Unidentified Complex Mixtures (UCM's)
21	28.749	2.337	Unidentified Complex Mixtures (UCM's)
22	29.046	2.195	Unidentified Complex Mixtures (UCM's)
23	29.404	1.087	Unidentified Complex Mixtures (UCM's)
24	29.564	0.846	Unidentified Complex Mixtures (UCM's)
25	29.689	1.391	Unidentified Complex Mixtures (UCM's)
26	29.834	0.756	Unidentified Complex Mixtures (UCM's)
27	30.119	0.765	Unidentified Complex Mixtures (UCM's)
28	30.524	1.042	Unidentified Complex Mixtures (UCM's)
29	30.854	1.202	Unidentified Complex Mixtures (UCM's)
30	31.020	0.982	Unidentified Complex Mixtures (UCM's)

Table 4.12 GC/MS qualitative analyses showing the compounds identified in the DCM mixed with the Asphaltinic fraction of the crude oil that has undergone photodegradation using the Fe-TiO_2 photocatalyst.

#	Retention Time (RT)	Area %	Name of Compound
1	6.070	0.685	Tridecane
2	7.340	1.198	Tetradecane
3	7.736	0.509	Naphthalene 1,7 dimethyl

4	7.801	0.799	2,6,10 trimethylundecanoic Acid 2,2,2 triflouro ethyl ester
5	8.086	0.911	Heptadecane 2,6,10,14-tetramethyl
6	8.856	1.946	Tetradecane
7	9.261	0.485	4-Bromobutanoic acid tetra decyl ester
8	9.771	2.075	Hexadecane
9	10.307	1.246	Pentadecane 2,6,10 trimethyl
10	10.947	5.797	Heptadecane 2,6,10,14 tetramethyl
11	12.002	1.523	Nonadecane
12	12.072	1.319	Hexadecane 2,6,10,14-tetramethyl
13	13.048	1.516	Nonadecane
14	13.293	0.566	5,8,11,14-Eicosatetraynoic acid
15	14.033	1.493	Eicosane
16	14.978	1.485	Nonadecane
17	15.889	1.728	Octacosane
18	16.829	1.907	Heneicosane
19	17.960	2.190	Octacosane
20	19.270	1.891	Octacosane
21	20.596	2.047	Octacosane
22	21.936	1.763	Heptacosane
23	23.277	1.420	Heptacosane
24	24.592	1.025	Octadecane 3-ethyl-5-(2-ethylbutyl)
25	25.883	0.930	Octadecane 3-ethyl-5-(2-ethylbutyl)
26	26.583	0.822	UCM’s
27	27.253	0.942	Octadecane 3-ethyl-5-(2-ethylbutyl)
28	27.573	0.834	UCM’s
29	27.794	0.998	Phenanthrene-9-dodecyltetradecahydro

30	28.879	0.663	UCM's

Table 4.13 GC/MS qualitative analyses showing the compounds identified in the DCM mixed with the asphaltinic fraction of the crude oil that has undergone photodegradation using the TiO_2 photocatalyst.

#	Retention Time (RT)	Area %	Name of Compound
2	7.800	0.827	Naphthalene 1,7 dimethyl
3	8.581	0.880	Pentadecane
4	9.026	0.798	Naphthalene 1,6,7 trimethyl
5	9.106	0.739	Naphthalene 1,6,7 trimethyl
6	9.496	1.130	Naphthalene 1,6,7 trimethyl
7	9.781	1.476	Naphthalene 2,3,6 trimethyl
8	10.717	0.775	Chamazulene
9	10.942	2.626	Hexadecane 2,6,10,14-tetramethyl
10	11.157	1.379	9H-flourene 2-methyl
11	11.437	0.996	1,4,5,8-tetramethylnaphthalene
12	12.442	0.940	Phenanthrene 9,10 dihydro-1-methyl
13	13.298	0.880	Iriccyclo[.7,4.1.1(2,7)] pentadeca-2,4,6,9,11,13-hexadecane-8-ol

14	13.548	1.048	Naphtho[3,4:2,3]bornene
15	14.038	0.919	Heptadecane 9-hexyl
16	14.563	1.178	Phenanthrene 3,6-dimethyl
17	14.638	0.832	Phenanthrene 2,7-dimethyl
18	15.674	0.819	Phenanthrene 2,3,5 trimethyl
19	15.899	1.543	Heptadecane 9-hexyl
20	16.834	1.664	Heptadecane 9-hexyl
21	17.980	2.079	Heptacosane
22	19.275	2.031	Pentacosane
23	20.606	2.013	Heptacosane
24	21.956	1.514	Octacosane
25	23.292	1.196	Heptacosane
26	24.612	1.222	Octadecane 3-ethyl-5-(2-ethylbutyl)
27	25.898	0.914	Tetrapentacontane 1,54-dibromo
28	26.488	0.984	UCM’s
29	26.588	0.811	Alfa.21a-28-30-Binorhopane
30	27.563	0.769	UCM’s

Table 4.14 GC/MS qualitative analyses showing the compounds identified in the paraffinic fraction of the crude oil that has not undergone degradation.

#	Retention Time (RT)	Area %	Name of Compound
1	3.644	0.708	Undecane
2	4.819	1.533	Dodecane
3	4.969	0.734	1-Octanol-2-butyl
4	5.710	1.147	Dodecane 4,6 dimethyl
5	6.075	1.857	Tridecane
6	6.190	0.637	Benzocycloheptatriene
7	7.030	0.805	Dodecane 2,6,10 trimethyl
8	7.125	1.250	Dodecane 2,6,10 trimethyl
9	7.345	2.384	Decahydro-4,4,8,9,10 pentamethylnaphthalene
10	7.745	0.688	Tetradecane
11	7.800	1.606	Naphthalene 1,8-dimethyl
12	8.091	1.422	Decahydro-4,4,8,9,10 pentamethylnaphthalene
13	8.271	1.339	Dodecane 2,6,10 trimethyl
14	8.856	2.695	Decahydro-4,4,8,9,10 pentamethylnaphthalene
15	9.776	2.213	Pentadecane
16	10.306	1.503	Hexadecane
17	10.952	5.699	Pentadecane 2,6,10 trimethyl
18	12.007	1.458	Pentadecane 2,6,10,14 tetramethyl
19	12.072	1.422	Octadecane
20	13.048	1.419	Hexadecane 2,6,10,14 tetramethyl
21	14.038	1.470	Nonadecane
22	14.988	1.527	Eicosane
23	15.894	1.770	Hexacosane

24	16.829	1.804	Hexacosane
25	17.964	1.786	Hexacosane
26	19.270	1.659	Hexacosane
27	20.595	1.464	Hexacosane
28	21.963	1.372	Heptacosane
29	23.272	0.993	Tetratetra contane
30	24.592	0.648	Ethanol 2- octadecyloxy

Table 4.15 GC/MS qualitative analyses showing the compounds identified in the DCM mixed with the paraffinic fraction of the crude oil that has undergone photodegradation using the Fe-TiO2 photocatalyst.

#	Retention Time (RT)	Area %	Name of compound
1	9.766	0.391	Nonadecane
2	10.902	0.683	Tert-Hexadecanethiol
3	10.937	0.602	Butane 2,2 dimethyl
4	13.738	0.439	Octadecanol 2-bromo
5	13.828	0.381	2-Nonadecanone 2,4 dimitrophenylhydrazine
6	14.028	0.496	Nonadecane
7	14.978	0.981	Nonadecane
8	15.899	1.834	Heneicosane
9	16.824	2.369	Hexacosane
10	17.965	2.615	Heptacosane
11	18.770	0.437	UCM’s
12	19.260	2.756	Eicosane 2-methyl
13	19.740	0.419	UCM’s
14	20.591	2.643	Octadecane 3-ethyl-5-(2-ethylbutyl-)
15	21.963	2.543	Octadecane 3-ethyl-5-(2-ethylbutyl-)

16	23.272	2.099	Octadecane 3-ethyl-5-(2-ethylbutyl-)
17	23.452	0.659	UCM's
18	24.587	1.414	Octadecane 3-ethyl-5-(2-ethylbutyl-)
19	25.903	0.403	UCM's
20	27.133	0.686	UCM's
21	27.248	0.613	UCM's
22	27.303	0.384	UCM's
23	27.328	0.431	UCM's
24	27.483	0.540	UCM's
25	27.523	0.460	UCM's
26	27.593	0.472	UCM's
27	27.793	0.899	UCM's
28	28.439	0.442	UCM's
29	29.799	0.390	UCM's
30	30.325	0.397	UCM's

Table 4.16 GC/MS qualitative analyses showing the compounds identified in the DCM mixed with the paraffinic fraction of the crude oil that has undergone photodegradation using the TiO_2 photocatalyst.

#	Retention Time (RT)	Area %	Name of Compound
1	8.578	0.900	Nonadecane
2	9.771	1.164	Nonadecane
3	10.301	0.753	Dodecane 2,6,10 trimethyl
4	10.912	2.340	Nonadecane
5	10.947	2.340	Butanoic acid, 2-methyl 5-oxo-1-cyclopenten-1-yl ester
6	12.002	0.828	Nonadecane

7	13.037	0.881	Nonadecane
8	14.033	0.917	Octadecane, 2-methyl
9	14.978	1.065	Nonadecane
10	15.889	1.394	Heptacosane
11	16.829	1.687	Nonadecane
12	17.959	2.122	Octadecane, 2- methyl
13	19.265	2.408	Nonadecane
14	20.590	2.489	Methoxyacetic acid, 3-tetradecyl ester
15	21.941	2.762	Octacosane
16	23.277	2.296	Octacosane
17	24.597	1.634	Octadecane, 3-ethyl-5-(2-ethylbutyl)
18	25.893	1.723	Octadecane, 3-ethyl-5-(2-ethylbutyl)
19	26.128	0.883	UCM's
20	26.468	2.029	UCM's
21	26.588	1.415	Alfa.,21a-28,30-Bisnorhopane
22	26.868	0.999	UCM's
23	27.263	2.099	Octadecane, 3-ethyl-5-(2-ethylbutyl)
24	27.448	0.733	UCM's
25	27.573	1.873	Alfa.,21a-28,30-Bisnorhopane
26	27.798	1.755	Alfa.,21a-28,30-Bisnorhopane
27	28.469	0.870	UCM's
28	28.894	1.392	17-Pentatriacontene
29	29.474	1.099	UCM's
30	30.880	0.723	UCM's